University of Stavanger

FACULTY OF SCIENCE AND TECHNOLOGY

Bachelor's Thesis

Study program/specialization: Petroleum Engineering/ Drilling Technology	Spring/Autumn semester, 2021 Open
Author: Eline Jacobsen Vikse Haakon Skogstad	Haakon Skogstad Eline J. Vikse (Signature of author)
Program coordinator: Supervisor(s): Mesfin Belayneh.	
Title of bachelor thesis: ***NCS field data based New Density - velocity and compressional wave - Shear wave velocity models development: Empirical and Artificial NeuronNetwork based modelling*** Tittel på Norsk avhandling: Utvikling av ny tetthets - hastighet og kompresjon - skjærbølgehastighetsmodell basert på NCS-feltdata: Empirisk og kunstig neuronettverksbasert	
Credits: 20	
Keywords: Well modelling, sonic velocity, bulk density, data fitting	Number of pages: 67 + Supplemental material/other: 8 Stavanger, ……15-05-/2021…… Date/year

Acknowledgements

We wish to show appreciation to our supervisor, Mesfin Belayneh Agonafer for providing education, guidance and patience, throughout this process. Without his support we would not be able to learn so much during this semester.

Furthermore, we wish to thank Andreas Hable for his help procuring the well log data.

This have been an exiting period, and we want to thank everyone that have contributed.

Abstract

This thesis presents the development of new density and velocity regression models (single and multivariate based) and artificial neural network (ANN) based modelling using wireline log data obtained from Barents Sea, Norwegian Sea and North Sea.

The prediction and the limitation of the models have been tested on the nearby, far and very far field datasets in the NCS. Moreover, the predicting accuracy of literature models have been tested and compared with the newly developed models. In the application the models have been illustrated for log estimation, reflection coefficient, Uniaxial compressive strength, Young's modulus and Poisson's ratio determination.

The results showed that:

- Multivariate regression models improved the prediction and was better than the single parameter-based models.
- The ANN based modelling further improved the prediction compared with the regression models.

The study discovers that the new models' predictions show better results than the literature models in most cases, when applying the model in the region from where the models are developed.

Table of Contents

List of Figures

List of tables

Abbreviations

NCS – Norwegian Continental Shelf
MPa – mega Pascal (10^6*)*
OBP – Overburden Pressure [MPa]
SG – Specific Gravity
UCS – Uniaxial Compressive Strength
ANN – Artificial Neural Network
B.Sc. – Bachelor of Science

Symbols

C_0 *– uniaxial compressive strength [MPa]*
E – Young's modulus [MPa]
G –Shear modulus [MPa]
L – length [m]
P_{wf} *– formation fracture pressure [MPa]*
P_p *– pore pressure [MPa]*
P_w *– well pressure [MPa]*
P_{pg} *– pore fluid pressure gradient [sg]*
R^2 *– coefficient of determination*
v_p *– sonic p-wave velocity [ft/s]*
v_s *– sonic s-wave velocity [ft/s]*
α *– Biot's constant*
ρ *– density [g/cm*^{3}*]*
γ *– inclination [rad]*
ν *– Poisson's ratio [ ]*
φ *– Porosity [ ]*
Δt *– transit time [µs/ft]*
σ *– stress [MPa]*
$\sigma_{x,y,z}$ *– components of normal stress [MPa]*
$\tau_{x,y,z}$ *– components of shear stress [MPa]*
$\sigma_{1,2,3}$ *– principal stresses [MPa]*
σ_h *– minimum horizontal stress [MPa]*
σ_v *– vertical/overburden stress [MPa]*
$\sigma_{tectonic}$ *– tectonic stress [MPa]*
σ_t *– tensile stress [MPa]*
σ_θ *– tangential stress [MPa]*
σ_z *– axial stress [MPa]*
σ_r *– radial stress [MPa]*

1 Introduction

This B.Sc. thesis presents well log based new empirical models with the field data obtained from Barents Sea, Norwegian Sea and North Sea. The regression models are based on both single and multiple variables. Density-Compressional velocity, Density-Shear velocity and Compressional velocity-Shear velocity models are developed. Density and velocity multivariate models include porosity. The models are tested on its own well, the nearby field and far field datasets. Moreover, the results are compared with literature models and models developed by previous students at the University of Stavanger. The study also presents machine learning based modeling, to improve density and velocity estimations.

1.1 Background and motivation

Prior to drilling operation, it is imperative to design the necessary engineering works properly. Among others, the well stability program is one of these designs. The well stability program allows to determine safe well pressure, which is bounded between the well collapse and well fracturing pressure. The well pressure is determined from the mud weight and the annular circulation pressure loss (ΔP) in the annulus. The effective circulation density is given as: (Rehm et al., 2013)

$$ECD\ (sg) = \rho_{static\ (sg)} + \frac{\Delta P(bar)}{0.0981 TVD(m)} \qquad Eq.\ 1.1$$

Where,

- ECD = The effective circulation density, sg
- ρ_{static} = Static mud weight, sg
- ΔP = Pressure loss in annulus, bar

During drilling, if the well pressure exceeds the fracture gradient, the well will be fractured. This results in a huge mud loss. On the other hand, if the well pressure is less than the collapse gradient the wellbore wall fragments collapse into the well, as a result of the mechanical induced drill string. This hinder circulation back to the surface as well as it makes drilling ahead difficult. Despite that great efforts have been made in the industry; the well instability issue is still challenging. Figure 1.1 shows typical well programs.

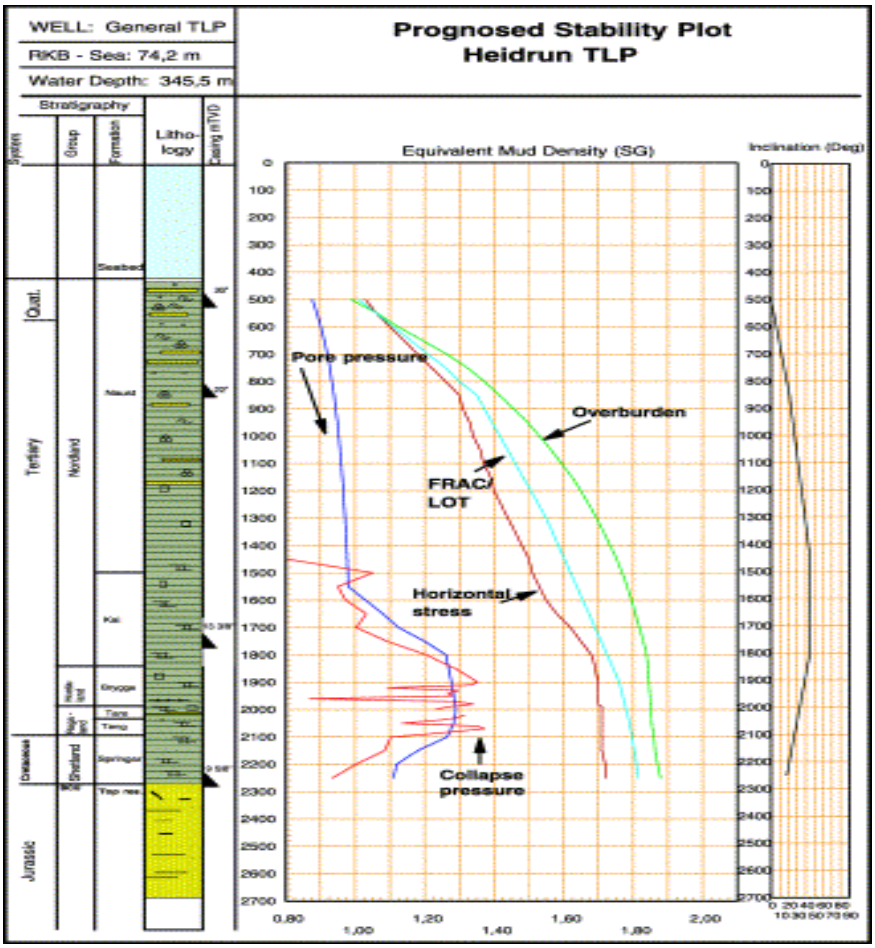

Figure 1.1: Well stability prognosis (Stjern et al., 2003)

The fracture pressure is the function of in-situ stress and pore pressure, as well as the tensile strength of the rock. The fracture pressure is also determined from Leak Off tests. As shown on the figure, Equinor (the former Statoil) estimate the collapse pressure from the Stati-Diaai failure criteria as provided in Eq. 1.2: (Stjern et al., 2003)

$$(\sigma_1 - \sigma_1)^2 + (\sigma_2 - \sigma_3)^2 + (\sigma_3 - \sigma_1)^2 = 2(C_o - T_o)(\sigma_1 + \sigma_2 + \sigma_3) + 2C_oT_o \qquad \text{Eq. 1.2}$$

Where,

- σ_1, σ_2 and σ_3 are the principal stress
- C_o is the uniaxial compressive strength (UCS)
- T_o is the tensile strength of the rock, which is normally assumed to be neglected since rocks consist of micro fractures

The stresses shown above will later be studied by relating them with the main tasks of this thesis.

UCS (C_o) is one of the important input parameters for the collapse modelling. It is practically impossible to quantify the formation UCS profile from the core samples extracted from the formation. This is because of cost, and the results would not be reliable since the core sample will lose its in-situ state of stress and fluids. Common practice at Equinor is that the UCS is estimated from the empirical correlation equation derived by Horsrud (Horsrud, 2001). Figure 1.2 show the estimation of the UCS compared with three test datasets, where one of the data showed discrepancy from the UCS-compressional wave Sonic correlation equation. It is important to use all the input parameters as accurate as possible for the design of well stability program. For instance, in the absence of compressional wave velocity, it is common practice to estimate such as Gardner (Gardner et al., 1974). Therefore, this thesis is designed to develop new models that may have potential to be used locally or in all of the Norwegian continental shelf.

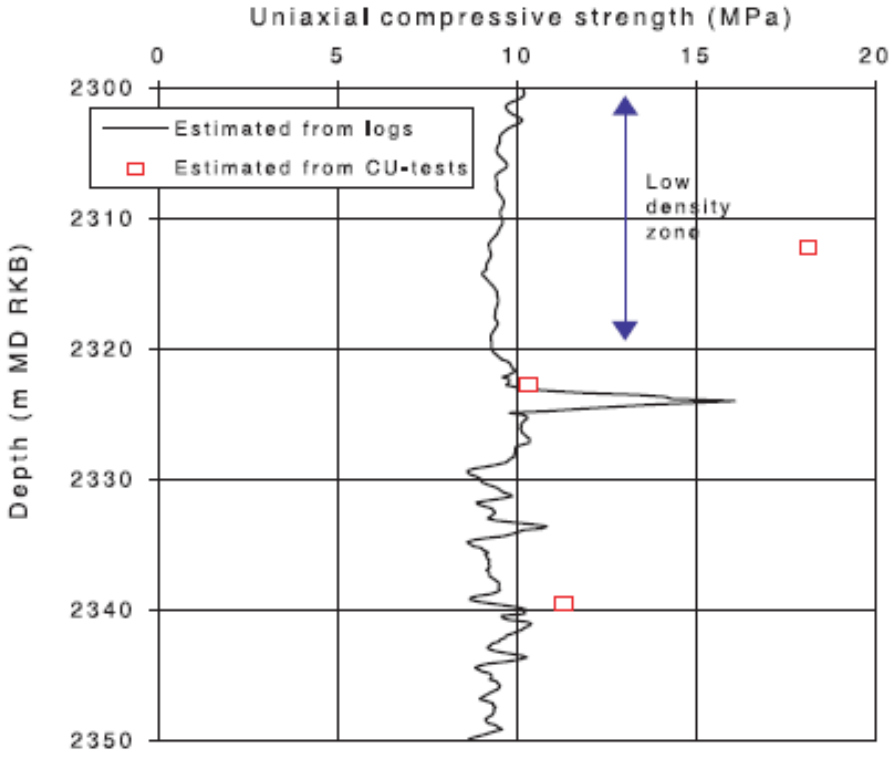

Figure 1.2: Comparison between the Uniaxial compressive strength predicted from sonic P-wave velocity and triaxial tests at three tested depths (Stjern et al., 2003).

1.2 Problem formulation

As described in the background part of the thesis, the well collapse and fracture models are calculated from in-situ stress, pore pressure, elastic and rock mechanical parameters. Most of the parameters are derived from well logs and seismic velocities of the formation.

For instance, the UCS as shown in Figure 1.2 is derived from the Horsrud's UCS – Compressional wave velocity model. However, the research questions to be addressed are:

1. In absence of compressional wave velocity or density logs, how good are the literature models; Gardner (Gardner et al., 1974), Castagna (Castagna et al., 1985), Anbazhagan (Anbazhagan et al., 2016) and Han (Han et al., 1986) to estimate the compressional wave velocity or density in the NCS? In other words, what is the application and the limitation of literature models in the NCS data predictions?
2. What is the application of the University of Stavanger B.Sc. students' models developed in previous years for the considered wells dataset?
3. What is the possibility of improving the previously developed models, with regard to reducing the error rate?

When it comes to empirical models, the application is not global, and one needs to test the model performance. Therefore, based on the NCS wireline log dataset new regression models (single parameters and multivariate based) will be developed and compared with the literature models. Moreover, machine learning based models will be modelled and the results compared with the empirical literature models and the newly developed regression models.

1.3 Objective

The objective of the study is to analyze the research questions addressed in section 1.2. The tasks are:

- To develop field data based empirical regression models
  - Compressional velocity (v_p) – Density (ρ)
  - Shear velocity (v_s) – Density (ρ)
  - Compressional velocity (v_p) – Shear velocity (v_s)
  - Compressional velocity as a function of density, shear velocity and porosity
  - Density as a function of compressional velocity, shear velocity and porosity
- To test the models on its own well, nearby fields and far fields to investigate the applicability and the limitation of the models.
- To compare the models with reviewed literature and UiS models.
- Artificial neural network (ANN) based modelling and compare the prediction with the regression-based modelling.
- Finally, to apply the model for geomechanics, drilling and geology fields.

1.4 Research methodology

Figure 1.3 shows the brief summary of the research method. The thesis' work comprises of three main parts. The first part deals with the literature studies of the parameters associated with the main work in the thesis. Well logging and empirical models are tested and compared with constructed models. Part two deals with modelling (Regression and Artificial neural network (ANN)), testing and comparisons. The last part deals with application of the model for geomechanics (UCS, E- and G-modulus), MSE/ROP, Geophysics fields.

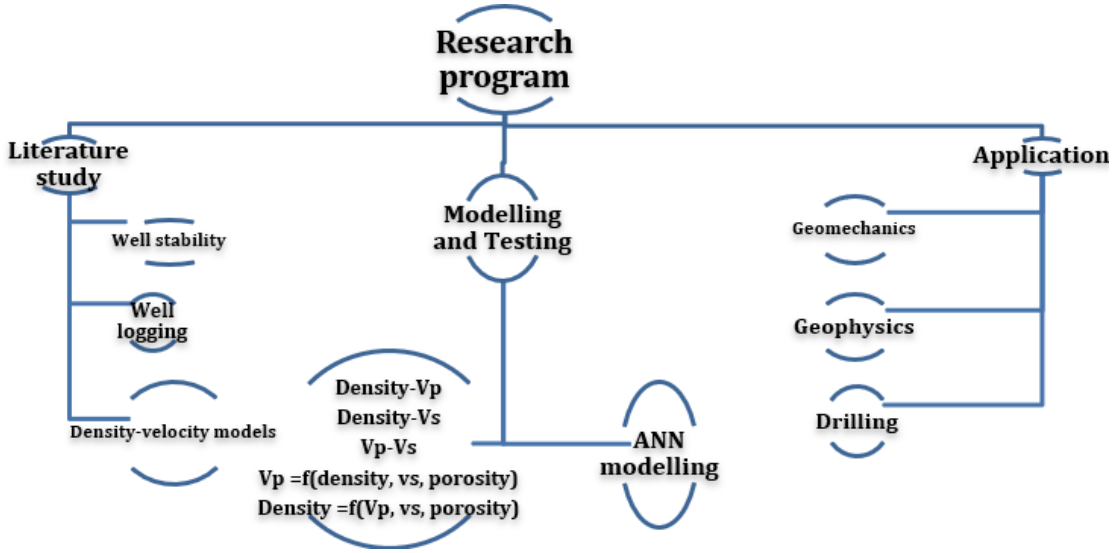

Figure 1.3: Research

2 Literature Study

This chapter is dedicated to present rock mechanical and elastic parameter determinations with respect to linking the importance of this study's model. In addition, the well log measurement principles are presented. Finally, the literature to be compared with the newly developed models are summarized. Designing an appropriate operational window is primarily dependent on the rock in-situ state, mechanical, elastic and formation pressure. As a result, designing the correct well pressure reduce the risk of well collapse, loss of circulation and reservoir fluid influx.

2.1 Stresses around a Wellbore

Before drilling the formation is in a state of stress, which are in the vertical and horizontal direction (maximum and minimum stresses). Figure 2.1 shows the directions of stresses with respect to an included wellbore (Manshad et al., 2014).

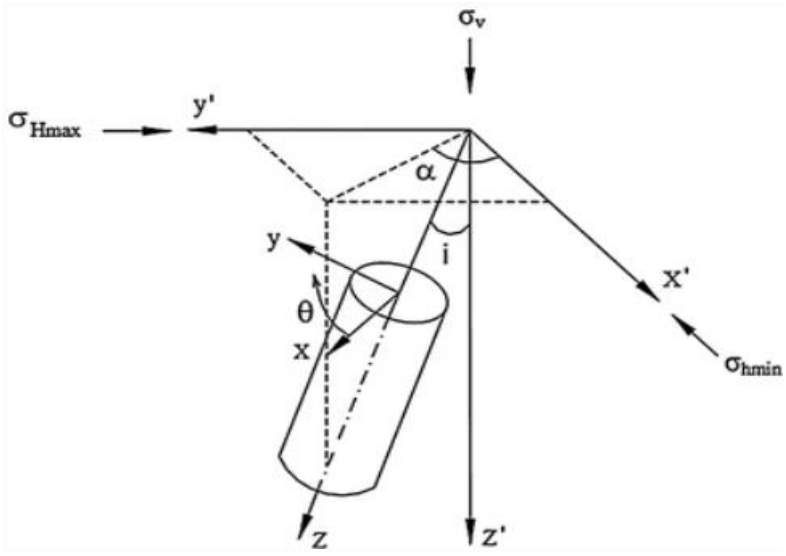

Figure 2.1: Inclined wellbore and the direction of in-situ stresses (Manshad et al., 2014)

Based on plain strain assumption Kirsch has solved the problem stress concentration around the wellbore for pressure loading and in-situ stresses. The detail of the modelling is beyond the scope of this study. The in-situ stresses can be transferred to the correct inclination (φ) and azimuth (γ). The normal and shear stress components can be expressed by principal stress system (σ_h, σ_H, σ_v) as: (Manshad et al., 2014)

$$\sigma_{xx} = (\sigma_h \cos^2\varphi + \sigma_H \sin^2\varphi)\cos^2\gamma + \sigma_v \sin^2\gamma \quad \textit{Eq. 2.1}$$

$$\sigma_{yy} = \sigma_h \sin^2\varphi + \sigma_H \cos^2\varphi \quad \textit{Eq. 2.2}$$

$$\sigma_{zz} = (\sigma_h \cos^2\varphi + \sigma_H \sin^2\varphi)\sin^2\gamma + \sigma_v \cos^2\gamma \quad \textit{Eq. 2.3}$$

$$\tau_{xy} = \frac{1}{2}(\sigma_H - \sigma_h)\sin 2\varphi \cos\gamma \quad \textit{Eq. 2.4}$$

$$\tau_{yz} = \frac{1}{2}(\sigma_H - \sigma_h)\sin 2\varphi \sin\gamma \quad \textit{Eq. 2.5}$$

$$\tau_{xz} = \frac{1}{2}(\sigma_h \cos^2\varphi + \sigma_H \sin^2\varphi - \sigma_v)\sin 2\gamma \quad \textit{Eq. 2.6}$$

For the sake of simplicity, let us assume a vertical well and isotropic stress state where the horizontal stresses are equal, the stress concentrations at the inner wall of the wellbore will be reduced to: (Manshad et al., 2014)

$$\sigma_r = P_w \quad \text{Eq. 2.7}$$

$$\sigma_\theta = 2\sigma_h - P_w \quad \text{Eq. 2.8}$$

$$\sigma_z = \sigma_v \quad \text{Eq. 2.9}$$

Where,

- σ_r = radial stress
- σ_θ = Hoop stress
- σ_z = axial stress
- Pw = well pressure
- σ_v = Overburden stress
- σ_h = Horizontal stress

2.2 Well stability

The two well failure mechanisms are tensile failure and shear failure, which results in well fracture and well collapse respectively. Figure 2.2 illustrates the schematics of the well pressure with respect to the wellbore condition (Zhang, 2013). On the figure, the green window is the safe operation, which needs to be designed prior to drilling operation. In literature several analytical methods and numerical models have been developed for borehole stability analyses. The commonly used methods will be reviewed in order to show the models capability to fill the gap in absence of a required dataset.

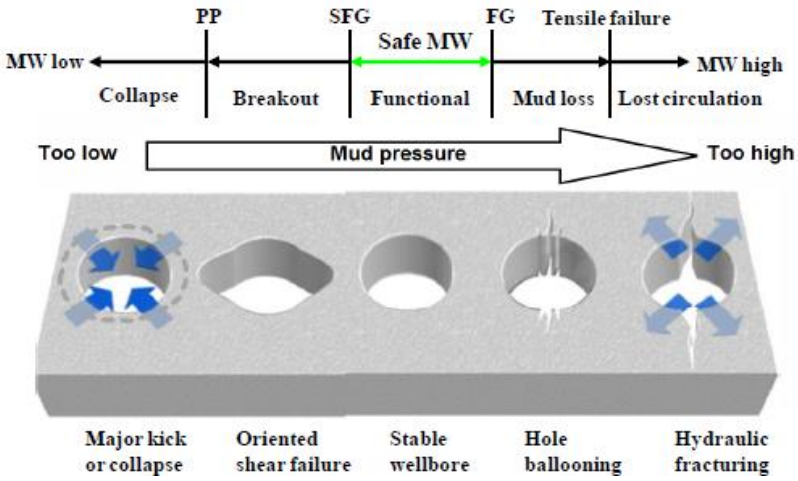

Figure 2.2: Wellbore failure schematics with respect to the wellbore pressure (Zhang, 2013)

2.2.1 Fracture model

The fracture pressure gradient is the higher bound on well stability program, such that the well pressure should not exceed the fracture pressure. Normally Leak Off Test is conducted right below the casing shoe to determine the fracture pressure. Based on the stress concentration, the fracture pressure is derived for penetrating and non-penetrating boundary conditions. Figure 2.3 shows the fracture wings in the direction of maximum horizontal stress.

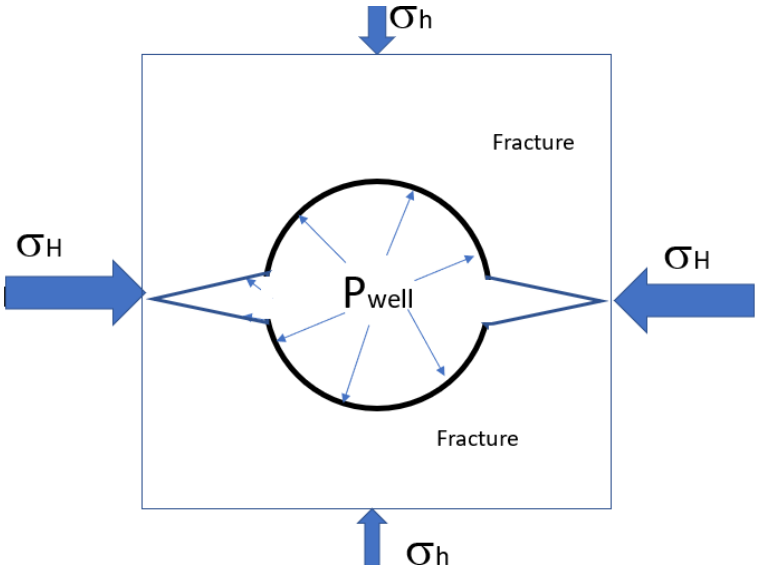

Figure 2.3: Well fracturing and fracture wings (Modified from(Fjar et al., 2008)

Non-penetrating boundary condition

The well pressure is not communicating with the formation pressure, as illustrated in Figure 2.4

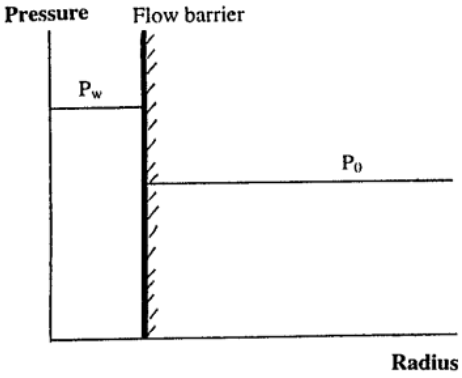

Figure 2.4: Non-Penetrating boundary condition (Aadnoy, 1998)

The fracture model for non-penetrating boundary condition is then given as: (Aadnoy & Looyeh, 2011)

$$P_{wf} = 3\sigma_h - \sigma_H - P_0 - \sigma_t \qquad \text{Eq. 2.10}$$

Where,

- σ_h and σ_H are the minimum and maximum in-situ horizontal stresses.
- Po is pore pressure.
- σ_t is tensile strength of the formation.

In sedimentary drilling formation, due to the presence of micro fractures, the tensile strength is very low, and assumed to be zero.

Based on volumetric strain, (Aadnoy & Looyeh, 2011)) have developed the complete fracture equation that couples temperature, Poisson's ratio, Youngs modulus as well as the plasticated yield strength of the formation. The model reads:

$$P_{wf} = \sigma_y + \frac{2(1+\upsilon)(1-\upsilon^2)}{2\upsilon(1-2\upsilon)(1+\upsilon)^2}\left\{\frac{3}{2}\sigma_x - \sigma_y - P_o\right\} + P_o + \frac{(1+\upsilon)^2}{2\upsilon(1-2\upsilon)(1+\upsilon)^2} E\kappa(T - T_{in}) + \frac{2}{\sqrt{3}} ln\left(1 + \frac{t}{a}\right) \qquad \text{Eq. 2.11}$$

Where,

- σ_x, σ_y are the in-situ stresses after being transformed for the given inclination and azimuth (see section 2.1, where $\sigma_{xx} = \sigma_x$, and $\sigma_{yy} = \sigma_y$),
- ν is Poisson ratio,
- E is Young's modulus,
- T is temperature,
- Po is formation pressure,
- Y is the yield strength of the formation,
- t is the plasticized zone of the formation and a is the size of the wellbore.

Penetrating boundary condition

Under the penetrating boundary condition, the well pressure is communicating with the formation pressure as illustrated in Figure 2.5.

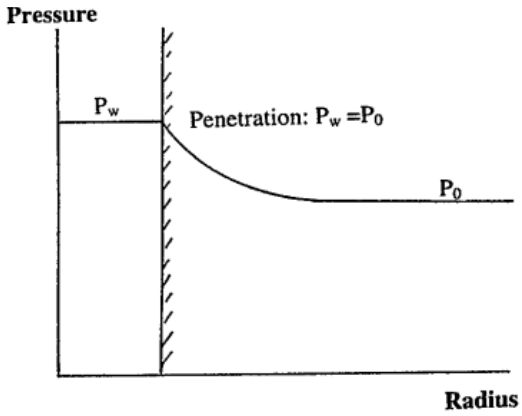

Figure 2.5: Penetrating boundary condition (Aadnoy, 1998)

From the figure, one can observe that well pressure is equal to formation pressure at the face of the wellbore. Setting this equality in Eq. 2.12, one can obtain the penetrating fracture pressure as: ((Aadnoy & Looyeh, 2011), p. 177)

$$P_{wf} = \sigma_h \qquad \text{Eq. 2.12}$$

Where,

- σ_h is the minimum horizontal stresses.
- Pw is fracture pressure

2.2.2 Collapse model

Unlike well fracturing, well collapse is the lower limit for the well pressure. For a safe drilling operation, the well pressure should be higher than the well collapse pressure. Figure 2.6 shows the well collapse in the direction of the minimum in-situ stress.

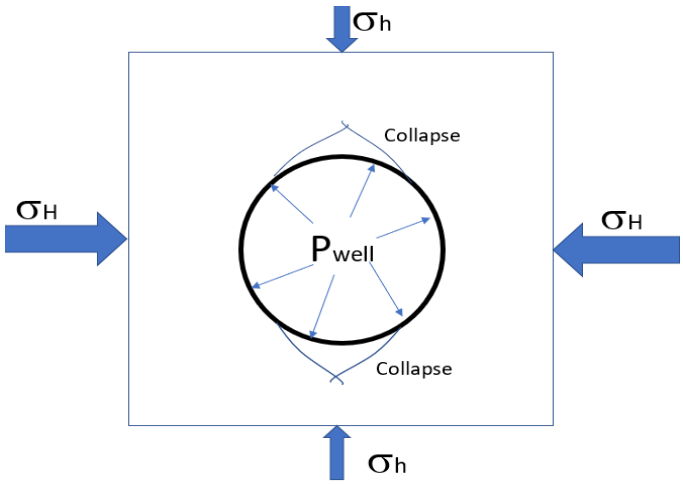

Figure 2.6: Well breakout at the minimum horizontal stress (Modified from (Fjar et al., 2008))

In literature, there are several well collapse failure criteria. As shown in Figure 1.1, the well collapse has been derived based on Stasi-di alia (Eq. 2.1). Among others, Mohr-Coulomb failure criteria is commonly used (Labuz & Zang, 2012). Based on the stress concentration, there are several borehole collapse pressure formulas (Fjar et al., 2008). Table 2.1 shows the collapse formulas under different stress state conditions:

Case	$\sigma_1 \geq \sigma_2 \geq \sigma_3$	Borehole failure occurs if	
a	$\sigma_\theta \geq \sigma_z \geq \sigma_r$	$p_w \leq P_f + \frac{2(\sigma_h - p_f) - C_0}{1 + tan^2\beta}$	*Eq. 2.13*
b	$\sigma_z \geq \sigma_\theta \geq \sigma_r$	$p_w \leq P_f + \frac{(\sigma_v - p_f) - C_0}{tan^2\beta}$	*Eq. 2.14*
c	$\sigma_z \geq \sigma_r \geq \sigma_\theta$	$p_w \leq P_f + 2(\sigma_h - p_f) - \frac{(\sigma_v - p_f) - C_0}{\tan^2\beta}$	*Eq. 2.15*

Table 2.1: Conditions for shear failure in vertical boreholes with isotropic far-field horizontal stresses and impermeable borehole wall (Fjar et al., 2008)

2.3 Description of Well stability model parameters

The input parameters for the fracture models and the collapse models presented in section 2.2.1 and 2.2.2 respectively are pore pressure, horizontal in-situ stresses, vertical (overburden) stress, Uniaxial compressive strength of the formation, internal friction angle and failure plane angle.

The models derived in this study will be used to determine these parameters. Therefore, this is the main motivation and application of the results obtained from the thesis. The following paragraphs describe the parameters.

2.3.1 Formation pressure

The formation or pressure, also called the pore pressure, is one of the parameters affecting the wellbore stability design. The parameter is commonly determined from empirical models based on seismic velocity in drilling formation, compressional velocity obtained from sonic logs and resistivity logs. The prediction depends on these parameters. However, logs are not usually available. Eaton (Eaton et al., 1975) derived an empirical model to determine the pore pressure from the density and sonic logs as:

$$P_{pg} = OBG - \left(OBG - P_{ng}\right)\left(\frac{\Delta t_n}{\Delta t}\right)^3 \quad \text{Eq. 2.16}$$

Where,

- Δt_n = the sonic transit time in shales at the normal Pressure, P_{ng}
- Δt = the sonic transit time in shales obtained from well logging,
- OBG = overburden gradient

This thesis' work is applied for the OBG in the absence of sonic travel time. Sonic travel time can also be inverted from the density log.

2.3.2 Overburden (vertical stress)

One of the principal stresses acting in the vertical downward direction is called the vertical or overburden stress, σ_v. The stress state at a given depth is determined from the weight of the overlying rock masses per unit area. In short, the vertical stress is calculated by integrating the density log over the depth z, as: (Karimi et al., 2014)

$$\sigma_v = \int_0^z \rho(z) * g \, dz \quad \text{Eq. 2.17}$$

Where,

- ρ = the density of each formatting having the thickness dz
- g = acceleration due to gravity
- z = depth.

Figure 2.7 shows an example of the calculation of overburden from the corresponding density log. The overburden is increasing with depth due to the sum of rock masses as depth increases.

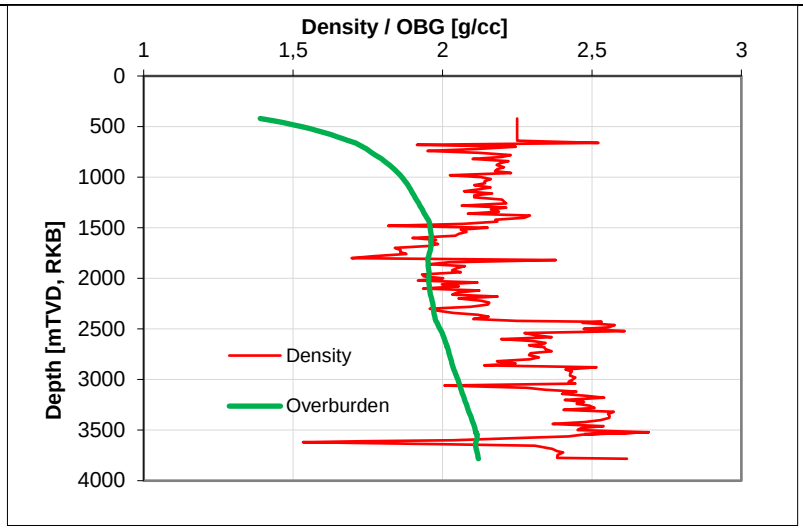

Figure 2.7: Determination of overburden from density

In absence of a density log, it is common practice to estimate density from the velocity log (ex. Gardner's equation). However, the issue is if Gardner's equation is good enough, as addressed in section 1.2. Therefore, this thesis' work is designed to fill the gap by analyzing the literature model as well as developing new improved models.

2.3.3 Horizontal stress

In tectonic relaxed region with regards to the isotropic stress state, the horizontal stresses are determined from overburden and pore pressure as: (Fjar et al., 2008)

$$\sigma_h = \frac{v}{1-v}\left(\sigma_v - \alpha * P_p\right) + \alpha * P_p \qquad \text{Eq. 2.18}$$

Where,

- σ_h = minimum horizontal stress,
- σ_v = overburden stress,
- P_p = pore pressure,
- α = Biot's constant (usually between 0.7-1),
- ν = Poisson's ratio.

Figure 2.8 shows an illustration of the determination of horizontal stress from the pore pressure and the overburden stress that has been calculated from a density log in Figure 2.7.

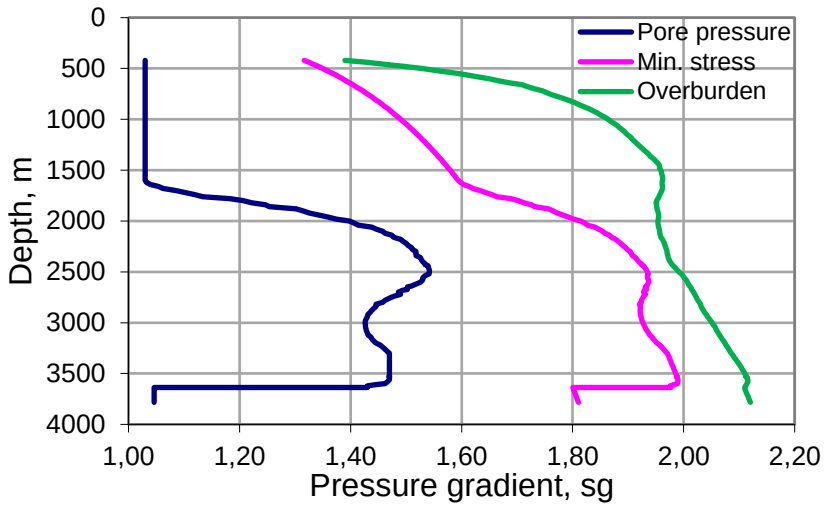

Figure 2.8: Determination of horizontal stress from the overburden and pore pressure

In absence of a density log it is required to use an empirical equation to estimate the density from velocity logs, this study provides a useful model for this occurrence.

2.3.4 Failure plane angle

As shown in the collapse equation, Figure 2.6, the failure angle of the rock is one of the input parameters. Normally, the failure plane angle (β) is determined from Uniaxial compressive stress test. It is related with the internal friction angle as: (Fjar et al., 2008)

$$\beta = \frac{\pi}{4} + \frac{\varphi}{2} \qquad \text{Eq. 2.19}$$

Where, φ is the angle of internal friction.

However, as mentioned, it is not possible to do laboratory tests for the drilling formation.

2.3.5 Internal friction angle

The common practice of determining internal friction angle of rock specimen is from several compressive datasets that include both Uniaxial and deviatoric tests. Using the datasets, one can generate more datapoints in order to delineate the failure zones. This is determined from the failure line, and the tangent inverse of the slope of the line describe internal friction angle (Fjar et al., 2008). However, this method of finding the internal friction angle for the drilling depth formation is practically impossible. Lal et al. have proposed a model that relates the internal friction angle with compressional wave velocity as: (Lal, 1999)

$$sin\varphi = \frac{V_p - 1}{V_p + 1} \qquad \text{Eq. 2.20}$$

To determine the internal friction angle and the failure plane angle, the input parameter is compressional wave velocity. In the absence of the sonic log, we can determine the compressional wave velocity from shear velocity or density logs. For this a good correlation equation is required. The correlation equations made in the thesis will be tested with literature models. Figure 2.9 shows an estimation of internal friction angle from sonic travel time.

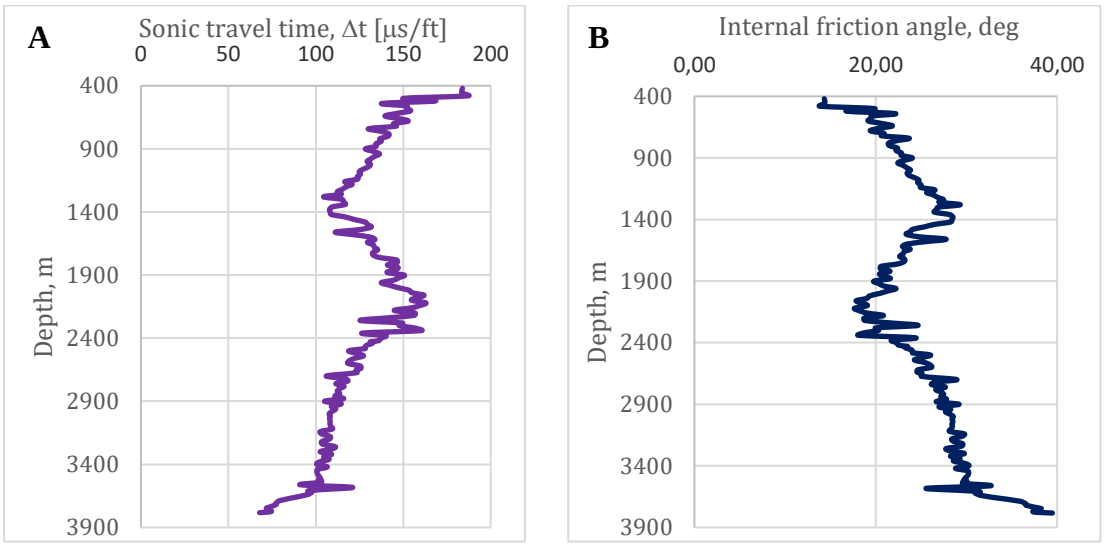

Figure 2.9: Estimation of internal friction angle (B) from sonic travel time (A)

2.3.6 Uniaxial compression strength

Uniaxial compressive strength of a rock describes the maximum load carrying capacity of the rock. It is the peak force of the laboratory destructive test. For the collapse modelling, as mentioned in section 2.2.2, Equinor is using empirical models that relate UCS with the compressional wave velocity. The model has been derived by Horsrud, based on shale rock specimens obtained from North Sea. However, in literature there are several UCV-VP based empirical models as well. In this thesis work we selected Horsrud's model (Horsrud, 2001) for the application. The model reads:

$$C_0 = 0{,}77 * v_p^{2{,}93} \qquad \text{Eq. 2.21}$$

where, C_0 is in MPa and, v_p is in km/s.

Lal (Lal, 1999) also developed a model, from high porosity Tertiary shale:

$$C_0(MPa) = 10\left(\frac{304.8}{\Delta t} - 1\right) \qquad \text{Eq. 2.22}$$

Where, Δt is sonic travel time (µs/ft).

It can be noted that the model requires sonic log data to compute the UCS. In absence of a sonic log, this thesis' models are designed to improve the estimation so that the UCS calculation is as accurate as possible.

Figure 2.10 displays the comparison between Lal (Lal, 1999) and Horsrud (Horsrud, 2001) model prediction. The different models predict differently. It is therefore important to compare models with measured data, as shown in Figure 1.2.

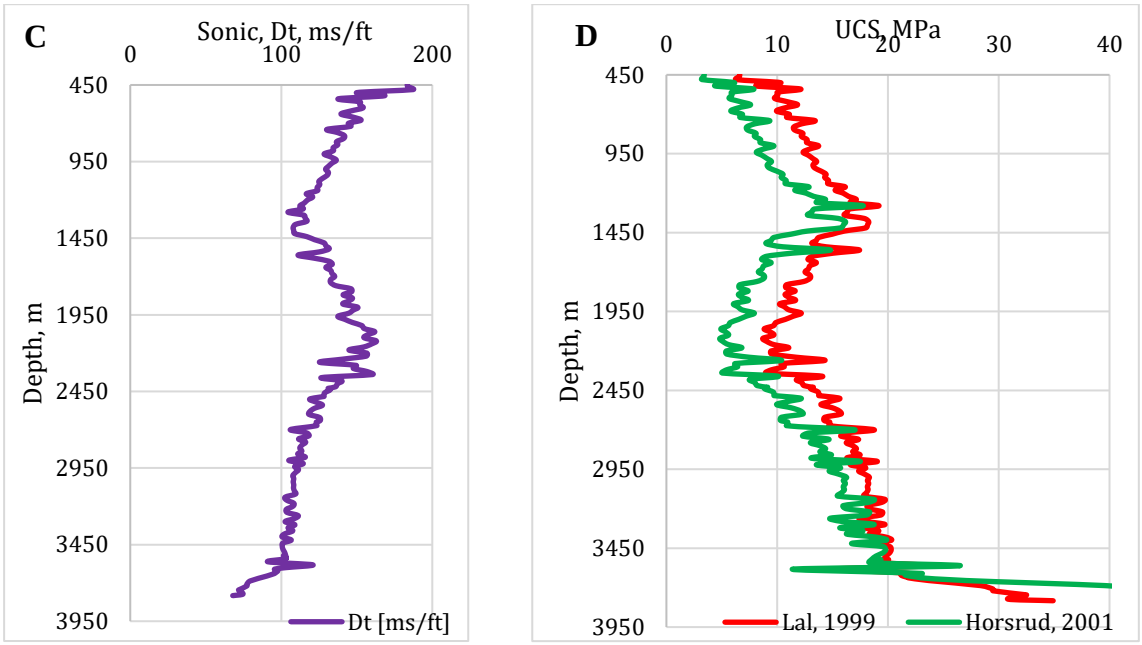

Figure 2.10: Comparison of UCS- predictions from sonic travel time (C) by Horsrud's and Lal's correlations (D).

Formations filled with water or hydrocarbon has large hydrogen content, the energy loss is higher. This indicates that the formation can be porous and filled with fluids. Figure 2.21 and Figure 2.22 display the typical Neutron porosity response of the formation Barents Sea and North Sea well data.

2.3.7 Young's modulus

As shown in the complete fracture equation (Eq. 2.11), the Young's modulus for the drilling formation is one of the input parameters. The parameter is normally determined from the mechanical Uniaxial compressive stress-strain curve, where the Hooke's law is valid (i.e. in the Linear elastic region)(Schmidt). As all other parameters, it is not practical to generate the Young's modulus as a profile. Here again, we use log based empirical models. Horsrud (Horsrud, 2001) has also developed the dynamic Youngs's modulus by relating with the compressional wave velocity as:

$$E = 0{,}076 v_p^{3{,}223} \qquad \text{Eq. 2.23}$$

Where, E is in GPa and v_p is in km/s.

2.3.8 Shear modulus

Similarly, Horsrud (Horsrud, 2001) has developed an empirical shear resistance of the drilling formation by relating with the compressional wave velocity as:

$$G = 0{,}03 v_p^{3{,}3} \qquad \text{Eq. 2.24}$$

Where, G is in GPa and V_p is in km/s.

2.3.9 Poisson's ratio

The Poisson's ratio is an important parameter for engineering design. As shown in well fracturing Eq. 2.11 and horizontal stress Eq. 2.18, the Poisson's ratio is an input parameter. The parameter is determined from the destructive mechanical uniaxial compressive strength test, by using the ratio of the transversal to the longitudinal strain.

The compressional wave velocity in terms of the bulk and shear modulus can be given as: (Fjar et al., 2008)

$$v_p = \sqrt{\frac{K + \frac{4}{3}G}{\rho}} \qquad \text{Eq. 2.25}$$

Where,

- K is the bulk modulus,
- G is the shear modulus,
- ρ is the density.

Similar to the compressional wave propagation in the formation, the shear wave velocity is related with the shear modulus as: (Fjar et al., 2008)

$$v_s = \sqrt{\frac{G}{\rho}} \qquad \text{Eq. 2.26}$$

In an isotropic and homogenous situation, with two known elastic parameters, the third elastic parameter can be determined. Using the elastic constant and the wave velocities, the Poisson's ratio can be estimated from the measured primary and secondary waves as: (Fjar et al., 2008)

$$v = \frac{\left(\frac{v_p}{v_s}\right)^2 - 2}{2\left[\left(\frac{v_p}{v_s}\right)^2 - 1\right]} \qquad \text{Eq. 2.27}$$

Where,

- v_p = p-wave velocity
- v_s = s-wave velocity

Figure 2.11 shows examples of Poisson's ratio determination from NCS dataset. The Poisson's ratio of the drilling formation is an input parameter to determine the horizontal stress (Eq. 2.18) and the fracture pressure (Eq. 2.11).

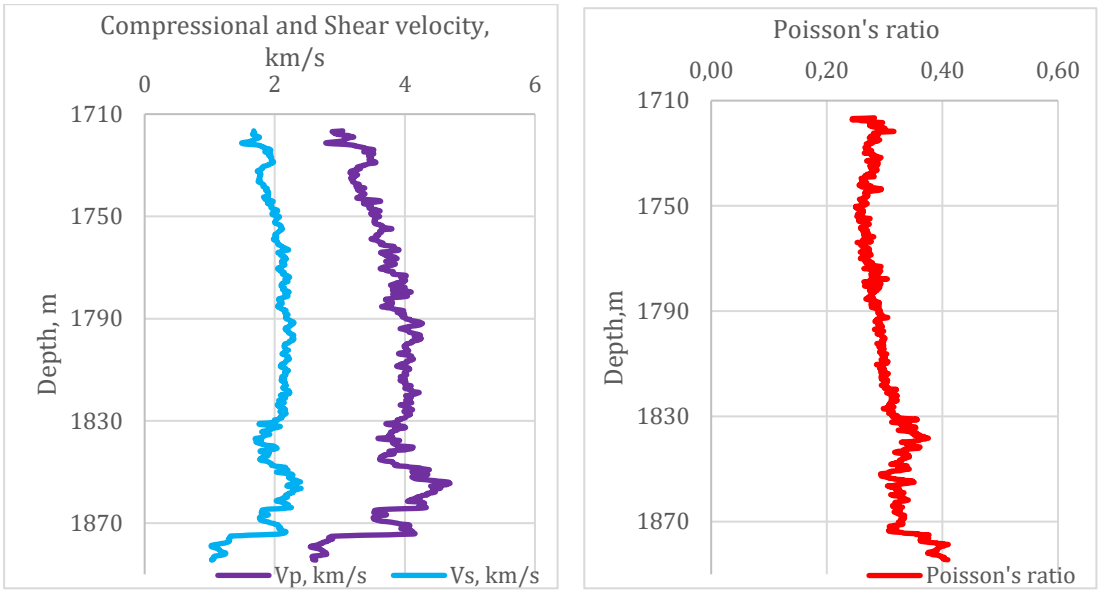

Figure 2.11: Estimation of Poisson ratio determination shear and compressional wave velocities of data obtained from the NCS.

It can be noted that the model requires sonic compressional and shear logs data to compute the Poisson's ratio of the formation. In the absence of one of the sonic logs, this thesis' work is designed to estimate the missing log data by developing improved empirical single and multivariate models.

2.4 Well Logging

In petroleum exploration, the formation properties are measured with logging tools. The information that well logs provide are formation thickness, formation tops, saturation of water, porosity, formation types, temperature, formation fluid types (water, oil and gas), formation pressure and formation dip.

Among the available logs obtained from the NCS, we have selected three logs that have shown correlation in literature. Therefore, measuring principles and the typical logs responses are presented in the following paragraphs.

2.4.1 Sonic Logs

Sonic logs measure the travel time by sending elastic waves into the formation and receiving the propagated waves at the receiver. The velocity of sound in the formation is calculated from the travel time and the distance between the source and the receiver. The waves travel time is often called slowness. Compressional (P-waves) and shear waves (S-waves) are two main types of seismic waves. P-waves travel faster and are therefore called primary waves. It can be transmitted through gas, liquid or solid material, and moves in a push-pull pattern. The secondary wave, S-waves, move in an up-down pattern. S-waves cannot propagate in liquids with zero/low viscosity. Figure 2.13 shows an illustration of sonic travel time measurement, as well as the different waves such as compressional and shear waves (Glover, 2000).

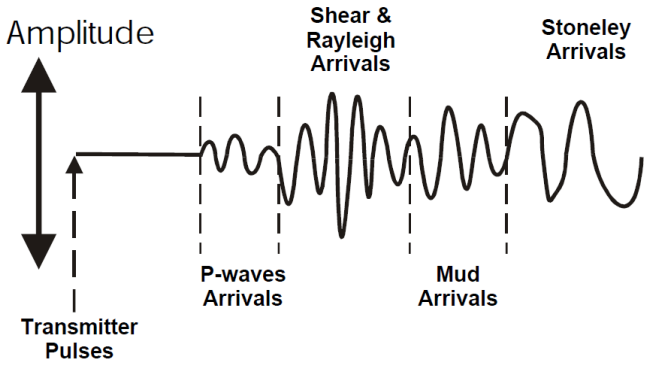

Figure 2.12: Geophysical wave trains received by a sonic log (Glover, 2000)

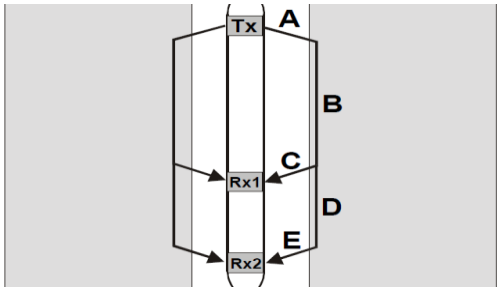

Figure 2.13: Dual receiver sonic tool (Glover, 2000)

Figure 2.14 and Figure 2.15 show the compressional and shear travel time data obtained from the Barents Sea and North Sea, respectively. As shown, the compressional (primary) wave is faster than the shear (secondary) wave.

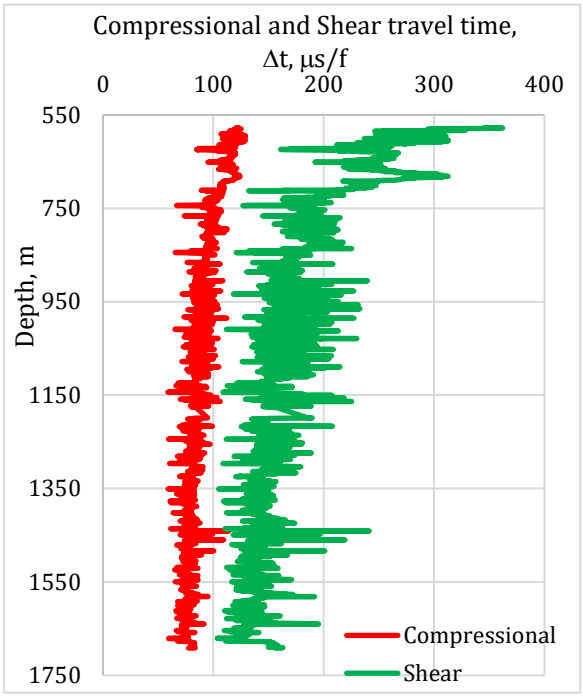

Figure 2.14: Compressional and Shear slowness log responses from Barents Sea

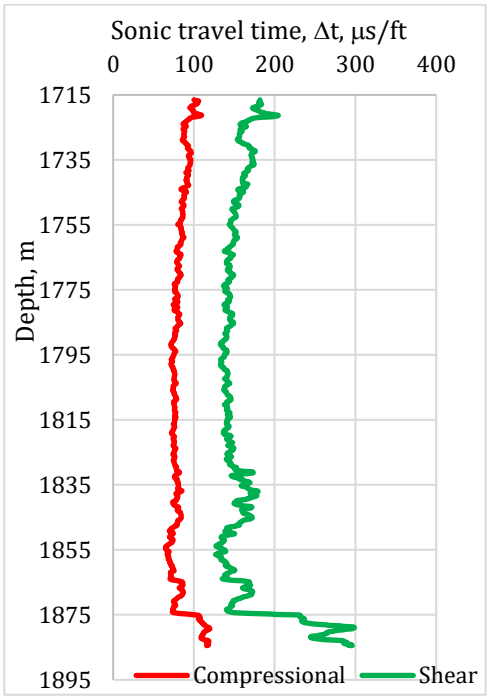

Figure 2.15: Compressional and Shear slowness log responses from North Sea

2.4.2 Density Logs

Density log is the logged result of the bulk density along the length of a borehole. Bulk density is dependent on different minerals, fluids and forces acting on the formation. The density log is measured with a gamma density tool, shown in Figure 2.16, that emits gamma ray at the source and records the gamma ray counts at the receiver which is placed a distance from the source. The interpretation is that the more gamma ray absorbed, it is associated with a denser formation. The gamma ray – electron collision is called Compton-scattering, as illustrated in Figure 2.17. The more electron density, results in more collisions.

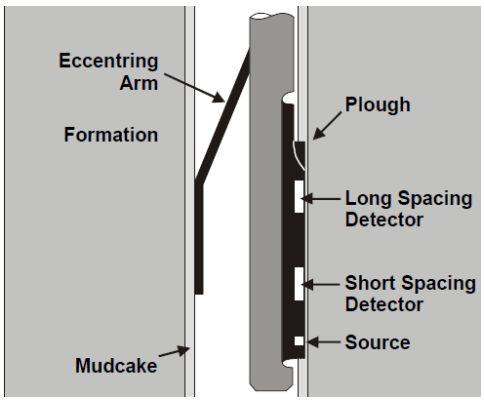

Figure 2.16: Density tool or Gamma ray density tool (Glover, 2000)

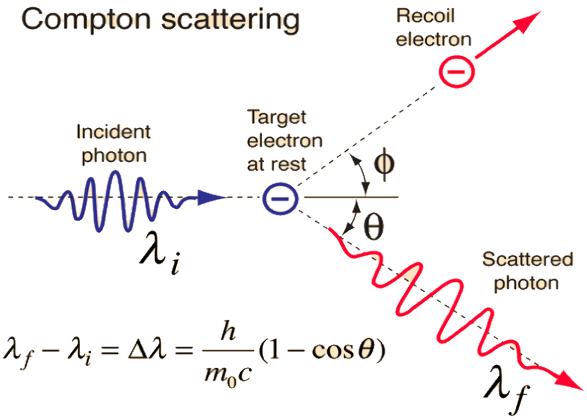

Figure 2.17: Compton scattering- Gamma ray collision with electron (Nave, 2021)

Figure 2.18 and Figure 2.19 are the density log data obtained from the Barents Sea and North Sea, respectively.

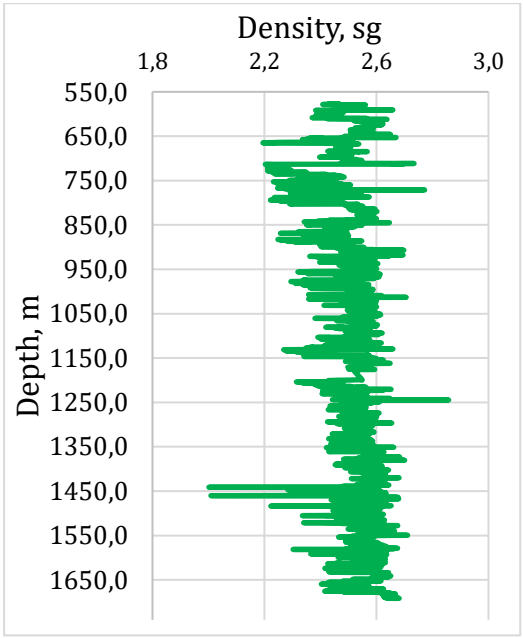

Figure 2.18: Density log from Barents Sea well

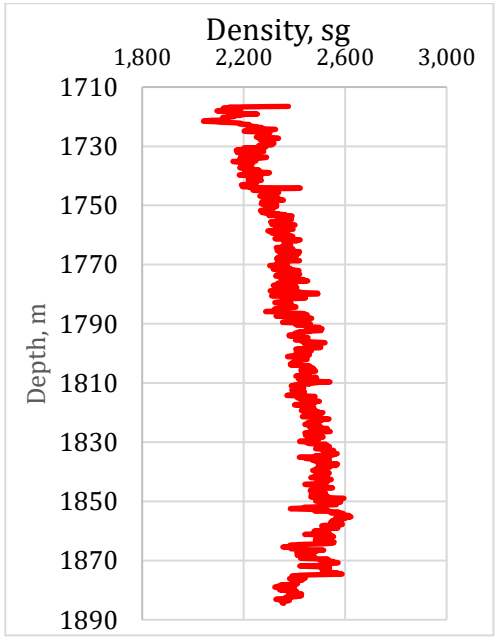

Figure 2.19: Density log from North Sea well

2.4.3 Neutron porosity log

The porosity of a formation is measured using well logs such as density log, acoustic logs and neutron logs. The porosity measuring principle neutron logs by quantifying the hydrogen content of the logged interval. This is done by counting the captured gamma ray or neutron counted at the detector. Figure 2.20 shows the emission of Neutrons from americium – beryllium mixture sources. Due to the collision of neutrons with formation nuclei, the neutrons lose energy.

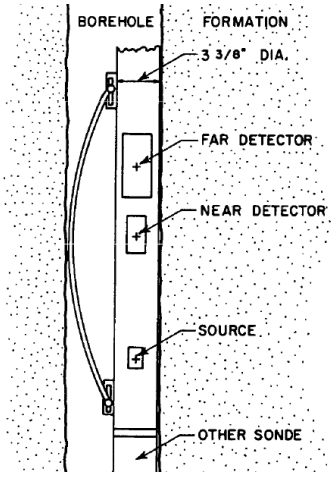

Figure 2.20: Dual-spacing Neutron (CNL) tool (Alger et al., 1972)

In formations filled with water or hydrocarbon there are large hydrogen content, and the energy loss is higher. This indicates that the formation can be porous and filled with fluids. Figure 2.21 and Figure 2.22 display the typical Neutron porosity response of the formation in Barents Sea and North Sea well data. Later, a multivariate regression based modelling technique will be used to model density as a function of compressional wave velocity and porosity of a formation.

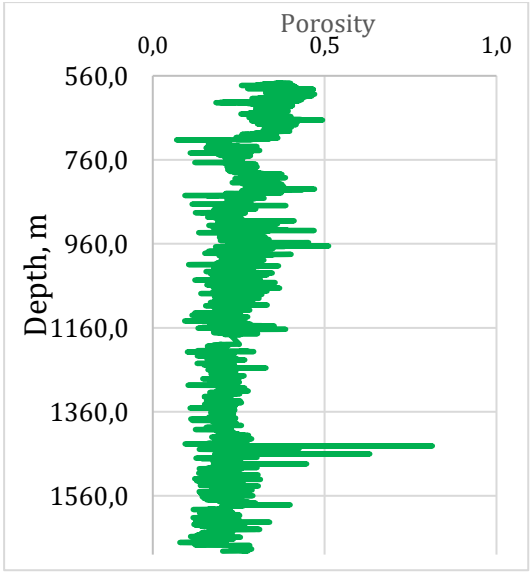

Figure 2.21: Example of neutron-log response from Barents Sea

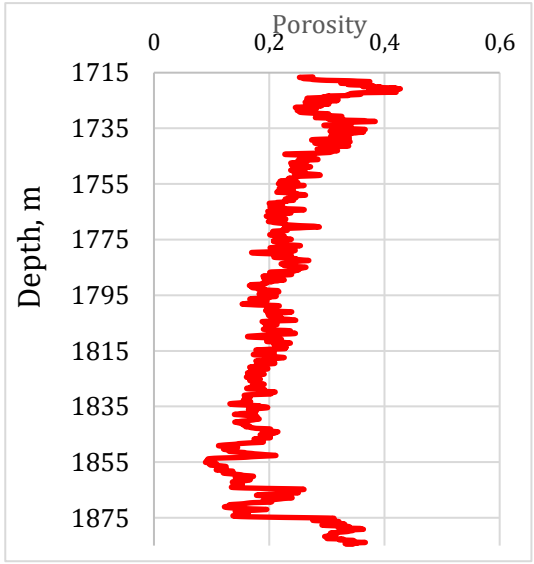

Figure 2.22: Example of neutron-log response from North Sea

2.5 Density-Velocity Empirical Models

Unlike physics-based modelling, empirical models are developed from experimental measured data. The correlation constants are not explicitly explained, but the physics that describe the physical phenomenon are embedded in the constants. The application of empirical modelling is conducted when the experimental data cannot be modelled thorough available physical laws. The application of the empirical modelling is found in every field of science. In the recent years, the application of data driven machine learning modelling is becoming more attractive, which developed among others regression equations that relate input with output. This approach is similar to the empirical modeling technique.

In literature there are several density-velocity empirical models that are developed based on laboratory and field measure data. In the following paragraphs both literature-based models and models developed at the University of Stavanger will be reviewed. The models are used for the analysis of NCS field dataset. Moreover, the reviewed models are compared with the models derived in this study.

2.5.1 Gardner's Model

Figure 2.23 shows density – velocity cross plots for several sedimentary rocks; Shale, Sandstone, Dolomite and Limestone. The data is from the Gulf of Mexico. From the same figure, it is possible to observe that the Salt and Coal deviates from the rest of the rock-types. However, Gardner (Gardner et al., 1974) developed a model relating density and velocity logs in a power law:

$$\rho = 0.23 v_p^{0.25} \qquad \text{Eq. 2.28}$$

Where, ρ is density (g/cm^3), the velocity is in ft/s and the empirical power law model constants are 0.23 and 0.25.

In terms of SI unit, v_p (in m/s) and density (in kg/m^3):

$$\rho = 310 v_p^{0.25} \qquad \text{Eq. 2.29}$$

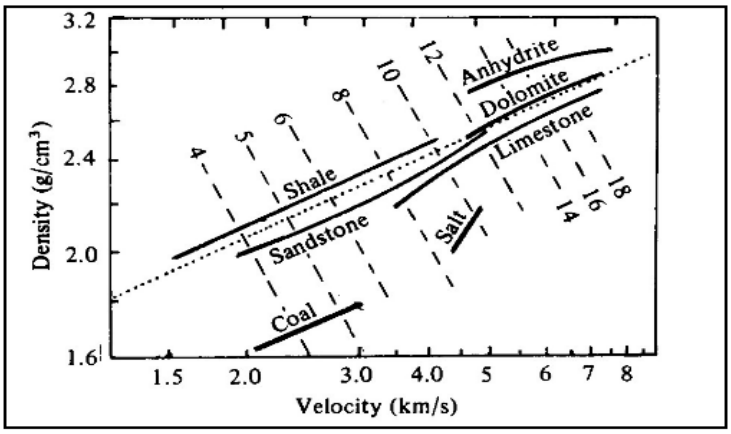

Figure 2.23: Gardner's Equation represented by dotted line (Nakoulima et al., 2004)

Gardner's equation is popular in hydrocarbon exploration. However, the applicability of the model for the NCS will be tested and compared with alternatives.

2.5.2 Petter Havnen's model (2020)

Petter (Havnen, 2020) developed two density - velocity models, using several modelling scenarios. The field data were obtained from the Barents Sea, Norwegian Sea and North Sea. The author reported the most accurate models for the continental shelf as:

$$\rho = -0{,}0612 * 10^{-9} * v_p^2 + 0{,}5795 * v_p + 1{,}1486 \quad \text{Eq. 2.30}$$

$$\rho = 1{,}7263 * v_p^{0{,}2645} \quad \text{Eq. 2.31}$$

Where, v_p is in ft/s.

2.5.3 Anbazhagan et. al's Model (2016)

Anbazhagan (Anbazhagan et al., 2016) developed an empirical model that relates the shear velocity (v_s) and density (ρ) data taken from 22 wells. The models are:

$$\rho = 0{,}779 * V_s^{0{,}158} \quad \text{Eq. 2.32}$$

$$\rho = 0{,}742 * V_s^{0{,}163} \quad \text{Eq. 2.33}$$

In this thesis, we will compare these models with the density – shear velocity models to be developed using the Norwegian continental shelf well data.

2.6 Compressional – Shear wave Velocity Empirical Models

2.6.1 Castagna et. al, 1985

Castagna (Castagna et al., 1985) coupled compressional velocity (v_p) and shear velocity (v_s) through linear empirical modelling. The models are based on water saturated silicate rock (i.e. sandstone, shale) datasets and the models read:

$$\boldsymbol{v_p} = 1{,}16 * \boldsymbol{v_s} + 1{,}36 \qquad \text{Eq. 2.34}$$

$$\boldsymbol{v_s} = 0{,}862 * \boldsymbol{v_p} - 1{,}172 \qquad \text{Eq. 2.35}$$

Where, Velocities (v_p and v_s) are in km/s.

About 75% of drilling formations are made up of shale. The model has been developed from data obtained from a region other than the NCS. Applicability of the model will be tested and compared with new models derived in this thesis.

2.6.2 Han et al. 1986

Han (Han et al., 1986) developed a shear velocity and compressional velocity model from extensive experimental dataset of sandstone. The dataset contained clay content variations, and a wide range of porosity. His study obtains the equation:

$$v_s = 0{,}794 * \ v_p^{0{,}787} \qquad \text{Eq. 2.36}$$

The estimations in this thesis model the compressional velocity from the shear velocity, therefore the Han model was inverted:

$$v_p = (\frac{v_s}{0{,}794})^{\frac{1}{0{,}787}} \qquad \text{Eq. 2.37}$$

This will be used to compare with the new empirical models.

3 Wellbore Database, Pre-processing and Modelling approach

In this section of the thesis modelling and approach of how the model results are made is presented and expounded. For density – compressional velocity, density – shear velocity, compressional velocity – shear velocity and then the multivariate models for density and compressional velocity. As well as the process of choosing the wells.

3.1 Well geography

Figure 3.1 show the map of Norway and the petroleum exploration basins. The well's data used for the modelling are from the Barents Sea, Norwegian Sea and the North Sea. As shown in Table 3.1, the wells are considered within a block. The main reason for the selection of the wells is to test the applicability of the models in local and far fields. By doing so, it would be easier to evaluate the limitation of the models.

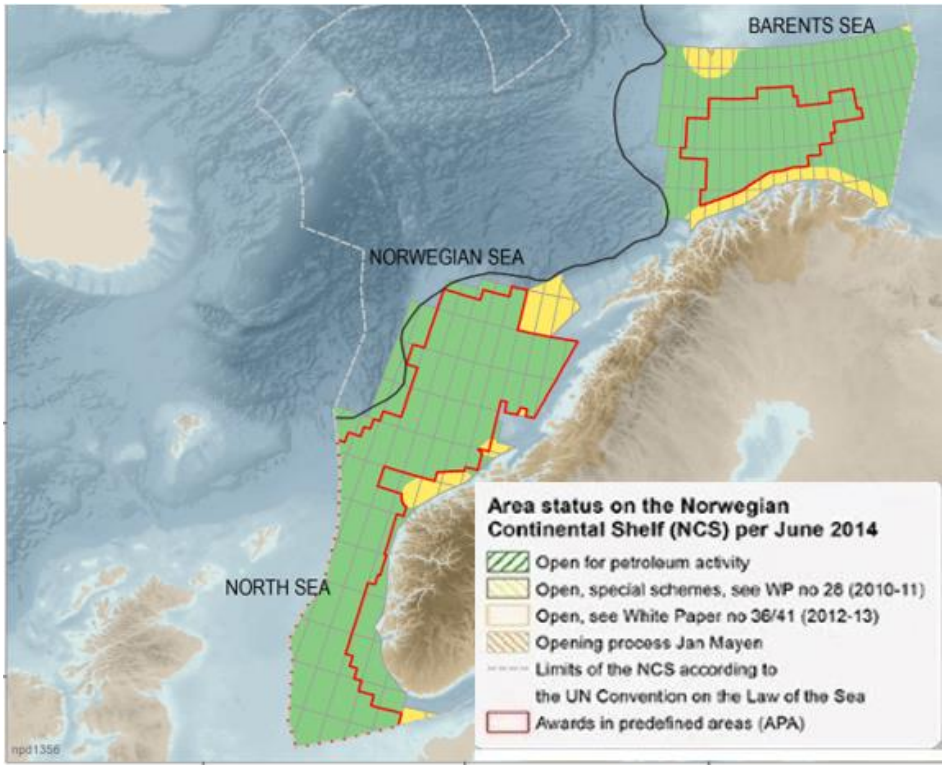

Figure 3.1: well locations in the Norwegian continental shelf (image, 2020)

North Sea	Norwegian Sea	Barents Sea
15-5-5	6608/10-17S	7124-3-1
15-6-12	6608/10-6	7125-1-1
16-2-3	6608/10-9	7324-6-1
16-2-4	6405/7-1	7324-7-2
16-2-6	6406/11-1S	7324-8-1
16-2-6T2		

Table 3.1: Norwegian continental shelf wells used for modelling and analysis

3.2 Data preparation

When receiving the data from the Diskos database, the format is .txt. The data is first converted into Excel. In the original data the value "-999,25" indicates that there was no recorded data, and it was therefore removed from the dataset before modelling.

The slowness data is in us/ft. The velocity is km/s, calculated as:

$$\frac{km}{s} = \frac{1}{\frac{us}{ft}} * 0{,}3048 * 10^3 \qquad \text{Eq. 3.1}$$

3.3 Regression models

The regression models are the relationship between a variable (x) and a scalar (y). Variables are the input, and the scalar is the output. For instance, predicting density log (output) from velocity log (input), is the main goal.

A linear regression model is a straight line, it has the equation: y = a*x + b, where the constants "a" and "b" are variables derived from the available data. As shown in Table 3.2, the other types of regression models, polynomial-, power-, exponential- and logarithmic-regression, has the same purpose as the linear regression.

Regression	Equation
linear regression	$y = a*x + b$
polynomial regression	$y = a*x^2 + b*x + c$
Power regression	$y = a*x^b$
Exponential regression	$y = a*e^{b*x}$
Logarithmic regression	$y = a*\ln(x) + b$

Table 3.2: Summary of regressions models to be used for modelling

The accuracy of the model is determined based on the correlation factor R^2, the model with the value closest to one is superior. A poor model has a R^2 value with a lower value.

Figure 3.2 illustrate this. The first figure show that the data concentration along a trend line and having R^2=0.90. The second graph show a scatter plot with a lower R^2 value of 0,50, the data points are spread further from the trend line. As shown in the third figure, R^2 =0.10, the data is even more dispersed and with this showing poor correlation.

During modelling, the datasets scalar and variables are plotted in order to select outliers from the datasets. By doing this, the modelling result would be improved.

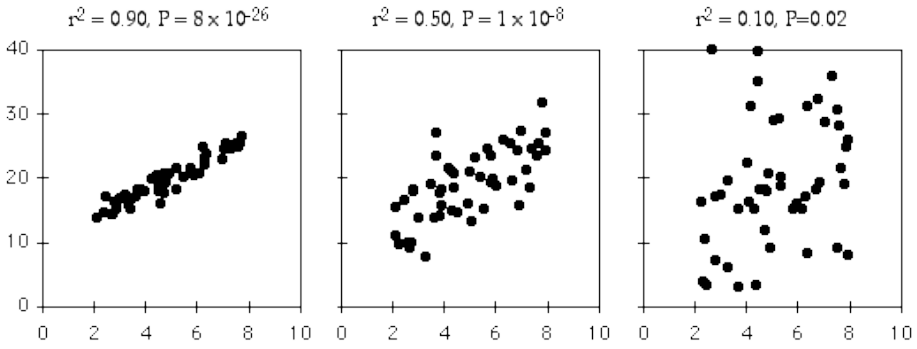

Figure 3.2: R-Squared values for different datasets (Mcdonald, 2015, July 20.)

3.4 Modelling Approach

The single variable models generated in this thesis are include:

- compressional velocity (v_p) – shear velocity (v_s)
- density (ρ) – shear velocity (v_s)
- density (ρ) – compressional velocity (v_p)

The multivariate regression models are based on:

- Density (ρ) – compressional velocity(v_p), shear velocity(v_s) and porosity(φ)
- Compressional velocity (v_p) - density(ρ), shear velocity(v_s) and porosity(φ).

The considered well data do not log all the necessary parameters to develop all the different models on every well. Table 3.3 shows the summary of the different models developed in the wells.

wells		ρ vs Vp	ρ vs Vs	Vs vs Vp	Vp = f (Vs, ρ,φ)	ρ = f (Vp. Vs, φ)
North Sea	15-5-5	√	-	-	-	-
	15-6-12	√	√	√	-	-
	16-2-3	√	√	√	√	√
	16-2-4	√	√	√	√	√
	16-2-6	√	√	√	√	√
	16-2-6T2	√	√	√	√	√
Norwegian Sea	6608/10-17S	√	√	√	-	-
	6608/10-6	√	-	-	-	-
	6608/10-9	√	-	-	-	-
	6405/7-1	√	-	-	-	-
	6406/11-1S	√	-	-	-	-
Barents Sea	7124-3-1	√	-	-	-	-
	7125-1-1	√	-	-	-	-
	7324-6-1	√	√	√	√	√
	7324-7-2	√	√	√	√	√
	7324-8-1	√	√	√	√	√

Table 3.3: Summary of correlation models developed for the different wells

After plotting the desired data in a scatter plot, the datasets were modelled with different regressions summarized in Table 3.2. In order to evaluate the predictive power of the models, an average percental error between the measured data and the model is calculated as:

$$Percentage\ error = \left\{\frac{1}{N}\sum_{1}^{N}\left|\frac{Measured\ data - \ model\ predicted}{Measured\ data}\right|\right\} * 100 \qquad \text{Eq. 3.2}$$

Where, N is the number of datasets.

4 Modelling Results and discussion

As mentioned, the modelling is based on linear, power, exponential, logarithmic and polynomial of the second order. This study's models that are presented in the tables below are the best models obtained from each well, which are selected based on R^2 value. All the models can be found in Appendix A 2.

4.1 Density – Compressional velocity

The density-shear velocity models developed are to be compared with Gardner's (Eq. 2.28) and Petter's (Eq. 2.30 and Eq. 2.31) models. Table 4.1, Table 4.2 and Table 4.3 are the density-velocity models for the North Sea, Norwegian Sea and Barents Sea wells. Most of the wells in the North Sea and Norwegian Sea show quite good correlation. In the Barents Sea, all the wells show poor correlation except for one of them.

North Sea wells	Model		R^2	Equation
15/5-5	Polynomial	$\rho = -0{,}1084V_p^2 + 0{,}8486V_p + 0{,}6658$	$R^2 = 0{,}4894$	Eq. 4.1
15/6-12	Polynomial	$\rho = -0{,}0442\ V_p^2 + 0{,}4249\ V_p + 1{,}5871$	$R^2 = 0{,}6677$	Eq. 4.2
16/2-3	Polynomial	$\rho = 0{,}1395\ V_p^2 - 0{,}8292\ V_p + 3{,}5254$	$R^2 = 0{,}5375$	Eq. 4.3
16/2-4	Polynomial	$\rho = -0{,}0426\ V_p^2 + 0{,}4591\ V_p + 1{,}3067$	$R^2 = 0{,}8218$	Eq. 4.4
16/2-6	Polynomial	$\rho = -0{,}0627\ V_p^2 + 0{,}5958\ V_p + 1{,}1134$	$R^2 = 0{,}7405$	Eq. 4.5
16/2-6T2	Polynomial	$\rho = -0{,}0552\ V_p^2 + 0{,}5485\ V_p + 1{,}1797$	$R^2 = 0{,}721$	Eq. 4.6

Table 4.1: The best density – compressional velocity models of North Sea wells

Norwegian Sea wells	Model		R^2	Equation
6608/10-17S	Polynomial	$\rho = 0{,}0501x^2 - 0{,}1971x + 2{,}6218$	$R^2 = 0{,}3383$	Eq. 4.7
6608/10-6	Polynomial	$\rho = -0{,}1242x^2 + 1{,}1284x + 0{,}0734$	$R^2 = 0{,}6371$	Eq. 4.8
6608/10-9	Polynomial	$\rho = -0{,}1821x^2 + 1{,}3634x - 0{,}1002$	$R^2 = 0{,}6362$	Eq. 4.9
6406/11-1S	Polynomial	$\rho = -0{,}1766x^2 + 1{,}294x + 0{,}1416$	$R^2 = 0{,}8017$	Eq. 4.10

Table 4.2: The best density – compressional velocity models of the Norwegian Sea wells.

Barents Sea wells	Model		R^2	Equation
7124/3-1	Polynomial	$\rho = -0{,}0358x^2 + 0{,}4506x + 1{,}3225$	$R^2 = 0{,}7241$	Eq. 4.11
7125/1-1	Polynomial	$\rho = 0{,}025x^2 + 0{,}0166x + 2{,}0457$	$R^2 = 0{,}2969$	Eq. 4.12
7324/6-1	Linear	$\rho = 0{,}0471x + 2{,}329$	$R^2 = 0{,}0464$	Eq. 4.13
	Polynomial	$\rho = -0{,}0013x^2 + 0{,}0565x + 2{,}3117$	$R^2 = 0{,}0464$	Eq. 4.14
7324/7-2	Polynomial	$\rho = 0{,}0566x^2 - 0{,}1487x + 2{,}5736$	$R^2 = 0{,}036$	Eq. 4.15
7324/8-1	Polynomial	$\rho = 0{,}0488x^2 - 0{,}2524x + 2{,}7604$	$R^2 = 0{,}0712$	Eq. 4.16

Table 4.3: The best density – compressional velocity models of the Barents Sea wells.

4.2 Density – Shear velocity

The density-shear velocity models developed are to be compared with Anbazhagan's models (Eq. 2.32 and Eq. 2.33). Norwegian Sea wells are presented in Table 4.5. Most of the wells in the North Sea (Table 4.4) show good correlation. On the other hand, the Barents Sea well data do not show correlation between density and shear velocity, with poor R^2 values (Table 4.6).

North Sea wells	model		R^2	Equation
15/6-12	Polynomial	$\rho = -0{,}2373V_s^2 + 1{,}1282\ V_s + 1{,}2696$	$R^2 = 0{,}4751$	Eq. 4.17
16/2-3	Polynomial	$\rho = 0{,}3396\ V_s^2 - 1{,}0372\ V_s + 3{,}096$	$R^2 = 0{,}2442$	Eq. 4.18
16/2-4	Polynomial	$\rho = -0{,}0438\ V_s^2 + 0{,}3801\ V_s + 1{,}8205$	$R^2 = 0{,}7547$	Eq. 4.19
16/2-6	Polynomial	$\rho = 0{,}0337\ V_s^2 - 0{,}0196\ V_s + 2{,}3132$	$R^2 = 0{,}2744$	Eq. 4.20
16/2-6T2	Polynomial	$\rho = 0{,}0539\ V_s^2 - 0{,}0522\ V_s + 2{,}3163$	$R^2 = 0{,}3831$	Eq. 4.21

Table 4.4: The best density – Shear velocity models made from the North Sea wells

Norwegian Sea wells	Model		R^2	Equation
6608/10-17S	Linear	$\rho = 0{,}1425\ V_s + 2{,}2753$	$R^2 = 0{,}2229$	Eq. 4.22
	Polynomial	$\rho = -0{,}0377\ V_s^2 + 0{,}2688\ V_s + 2{,}173$	$R^2 = 0{,}2238$	Eq. 4.23
	Power	$\rho = 2{,}3991\ V_s^{0{,}0924}$	$R^2 = 0{,}2267$	Eq. 4.24
	Exponential	$\rho = 2{,}2891e^{0{,}0555\ Vs}$	$R^2 = 0{,}2204$	Eq. 4.25
	Logarithmic	$\rho = 0{,}2364\ln(V_s) + 2{,}3961$	$R^2 = 0{,}2276$	Eq. 4.26

Table 4.5: The best density – Shear velocity models made from the Norwegian Sea wells

Barents Sea wells	Model		R^2	Equation
7324/8-1	polynomial	$\rho = 0{,}2265\ V_s^2 - 0{,}7066V_s + 2{,}9804$	$R^2 = 0{,}0461$	Eq. 4.27
7324/7-2	polynomial	$\rho = 0{,}0566V_s^2 - 0{,}1487V_s + 2{,}5736$	$R^2 = 0{,}036$	Eq. 4.28
7324/6-1	polynomial	$\rho = -0{,}0339V_s^2 + 0{,}1276V_s + 2{,}3837$	$R^2 = 0{,}0029$	Eq. 4.29

Table 4.6: The best density – Shear velocity models made from the Barents Sea wells

4.3 Compressional velocity – Shear velocity

Table 4.7, Table 4.8 and Table 4.9 show the results of the developed compressional–shear wave velocity regression models. The R^2 values are close to one in all three regions, which implies very good correlation. The best models are compared with literature models, such as Castagna's model, in chapter 5.

North Sea wells	Modell		R^2	Equation
15/6-12	Polynomial	$V_p = -0{,}197\ V_s^2 + 2{,}3202\ V_s + 0{,}0669$	$R^2 = 0{,}9038$	Eq. 4.30
16/2-3	Exponential	$V_p = 1{,}5192e^{0{,}4493\ Vs}$	$R^2 = 0{,}9468$	Eq. 4.31
16/2-4	Polynomial	$V_p = 0{,}04\ V_s^2 + 1{,}2842\ V_s + 1{,}0927$	$R^2 = 0{,}9840$	Eq. 4.32
16/2-6	Polynomial	$V_p = 0{,}2138\ V_s^2 + 0{,}5595\ V_s + 1{,}8256$	$R^2 = 0{,}8954$	Eq. 4.33
16/2-6T2	Polynomial	$V_p = 0{,}26\ V_s^2 + 0{,}459\ V_s + 1{,}8635$	$R^2 = 0{,}9538$	Eq. 4.34

Table 4.7: The best compressional velocity – Shear velocity models made from the Norwegian Sea wells

Norwegian Sea wells	Model		R^2	Equation
6608/10-17S	Linear	$y = 1{,}2537x + 1{,}1489$	$R^2 = 0{,}9566$	Eq. 4.35
	Polynomial	$y = 0{,}3413x^2 + 0{,}1363x + 2{,}0288$	$R^2 = 0{,}9622$	Eq. 4.36
	Power	$y = 2{,}3632x^{0{,}6213}$	$R^2 = 0{,}9582$	Eq. 4.37
	Exponential	$y = 1{,}6727e^{0{,}3914x}$	$R^2 = 0{,}9664$	Eq. 4.38
	Logarithmic	$y = 1{,}9793\ln(x) + 2{,}2599$	$R^2 = 0{,}9381$	Eq. 4.39

Table 4.8: The best compressional velocity – Shear velocity models made from the North Sea wells

Barents Sea	model		R^2	Equation
7324/8-1	Polynomial	$y = 0{,}3858x^2 - 0{,}0341x + 2{,}1783$	$R^2 = 0{,}7216$	Eq. 4.40
7324/7-2	Polynomial	$y = 0{,}0361x^2 + 1{,}1226x + 1{,}2659$	$R^2 = 0{,}9339$	Eq. 4.41
7324/6-1	Power	$y = 2{,}3871x^{0{,}6239}$	$R^2 = 0{,}8315$	Eq. 4.42

Table 4.9: The best compressional velocity – Shear velocity models made from the Barents Sea wells

4.4 Linear multivariate density and compressional velocity models

The single parameter-based density models presented above show variations between the wells. In general, the correlation is quite good for compressional velocity-shear velocity. Density-velocity models varies. In order to improve the correlation of the parameters this section presents both multivariate density and compressional velocity regression models.

Table 4.10 and Table 4.11 show the best multivariate regression models, in terms of R^2 value. The compressional velocity is a function of shear velocity, density and porosity, and the density is a function of compressional velocity, shear velocity and porosity. Results in general show that the linear multivariate regression models, have a higher R^2 value compared with the single parameter models. Since all the required datasets are not available in the Norwegian Sea, the table presents the linear multivariate model for the North Sea and Barents Sea only. The rest of the models can be found in Appendix A 2.

North Sea Wells	Multivariate model			R^2	Equation
16/2-3	Density	**ρ = a+bVp+ c*Vs +d*φ**	a = 2,49303316915152 b = -0,364520653041707 c = -1,11506204428424 d = 0,235156029285666	0,9027	Eq. 4.43
16/2-4	Velocity	**Vp = a+bVS+ c*ρ+d*φ**	a = 0,155316580102066 b = 1,15671991478187 c = 0,637287100100291 d = -0,582653091257998	0,9900	Eq. 4.44

Table 4.10: Multivariate density and compressional velocity from North Sea

Well Barents Sea	Multivariate model			R^2	Equation
7374/7-2	Velocity	**Vp = a+bVs+ c*ρ+d*φ**	a = -0.994025557751479 b = - 0.101369776327267 c = 1,17697879767033 d = 0.919461526349866	0,9628	Eq. 4.45
	Density	**ρ = a+bVp+ c*Vs +d*φ**	a = 1,66635205340664 b = 0,455362644344926 c = - 0,450285896817343 d = 0,388330919745864	0,4876	Eq. 4.46

Table 4.11: Multivariate density and compressional velocity from Barents Sea

5 Model testing and comparison

The models presented in Chapter 4 are tested on its own well, nearby wells (within its own sea), far field and very far field sea wells. For instance, the best North Sea model is tested on its own well (where the model has been derived from), and nearby wells within the North Sea, on far field wells in the Norwegian Sea and on very far field wells in the Barents Sea. The best models from the other seas are all tested in a similar manner. The main objective is to investigate the applicability and the limitation of the models compared with literature models reviewed in section 2.5 and 2.6. The percentage error deviation between the model and the data log for each of the datapoints are calculated. Considering the total average error percentage for each sea, this thesis' models are compared with the literature models.

5.1 Density – compressional velocity models

Results in Table 5.3 show that the Barents Sea model exhibits a reduced error deviation rate, except for the very far field well. Although Gardner's and Petter's models also predict the measured data quite well. Similarly, the model derived from the North Sea and the Norwegian Sea are tested and results are presented in Table 5.1 and Table 5.2. In Table 5.1 there is an exception, the model does not have the lowest error percentage in the North Sea wells even though this is the model's origin sea (it is marked with red text).

Model	Average error (%)			
	On its own well North Sea	*Nearby wells North Sea (%)*	*Far wells Norwegian Sea (%)*	*Very far wells Barents Sea (%)*
*This thesis (*Eq. 4.4*)*	2,444	3,831	6,206	5,756
*Gardner (*Eq. 2.28*)*	2,592	3,800	6,456	5,552
*Petter (*Eq. 2.31*)*	2,784	3,817	6,261	5,121

Table 5.1: Test of model derived from well 16/2-4, North Sea

Model	Average error (%)			
	On its own well Norwegian Sea	*Far wells North Sea (%)*	*Nearby wells Norwegian Sea (%)*	*Very far wells Barents Sea (%)*
This thesis (Eq. 4.10)	2,849	5,006	5,259	6,577
Gardner (Eq. 2.28)	4,290	3,800	6,456	5,552
Petter (Eq. 2.30)	3,598	3,926	5,864	5,316

Table 5.2: Test of model derived from well 6406/11-1s, Norwegian sea

Model	Average error (%)			
	On its own well Barents Sea	*Very far wells North Sea*	*Far wells Norwegian Sea*	*Nearby wells Barents Sea*
This thesis (Eq. 4.11)	3,319	4,164	5,917	4,364
Gardner (Eq. 2.28)	4,186	3,800	6,456	5,552
Petter (Eq. 2.31)	3,950	3,817	6,261	5,121

Table 5.3: Test of model derived from well 7124/3-1, Barents Sea

5.2 Density – shear velocity models

This thesis density-shear velocity models are shown, and compared with Abazhagan's models (Eq. 2.32 and Eq. 2.33), in Table 5.4, Table 5.5 and Table 5.6. The models exhibit a lower error rate for the region where the models has been developed. Well 6608-10-17S is the only well from the Norwegian Sea considered in the Density-Shear velocity model since the shear velocity data is not available for the other wells in the area.

Model	Average error (%)			
	On its own well North Sea	*Nearby wells North Sea*	*Far wells Norwegian Sea*	*Very far wells Barents Sea*
*This thesis (*Eq. 4.19*)*	2,972	3,798	7,609	6,505
Anbazhagan et. al (Eq. 2.32)	7,214	5,718	2,006	4,786
Anbazhagan et. al (Eq. 2.33)	5,864	4,863	2,620	4,753

Table 5.4: Test of model derived from well 16/2-4, North Sea

Model	Average error (%)			
	On its own well Norwegian Sea	*Far wells North Sea*	*Nearby wells Norwegian Sea*	*Very far wells Barents Sea*
*This thesis (*Eq. 4.26*)*	1,714	6,243	x	3,631
Anbazhagan et. al's (Eq. 2.32)	2,006	5,718	2,006	4,201
Anbazhagan et. al's (Eq. 2.33)	2,620	4,863	2,620	3,894

Table 5.5: Test of model derived from well 6608/10-17S, Norwegian Sea

Model	Average error (%)			
	On its own well Barents Sea	*Very far wells North Sea*	*Far wells Norwegian Sea*	*Nearby wells Barents Sea*
*This thesis (*Eq. 4.27*)*	3,462	7,238	2,794	3,581
Anbazhagan et. al's (Eq. 2.32)	4,495	5,718	2,006	4,786
Anbazhagan et. al's (Eq. 2.33)	4,207	4,863	2,620	4,753

Table 5.6: Test of model derived from well 7324/8-1, Barents Sea

5.3 Compressional velocity – shear velocity models

Average error for the compressional velocity-shear velocity models on the different seas, compared with Castagna's (Eq. 2.34) and Han's (Eq. 2.34) models are presented in Table 5.7, Table 5.8 and Table 5.9. This thesis models give better results for the nearby wells than the literature models commonly used. Again, the Norwegian Sea contains only one well.

Model	Average error (%)			
	On its own well North Sea	*Nearby wells North Sea*	*Far wells Norwegian Sea*	*Very far wells Barents Sea*
*This thesis (*Eq. 4.32*)*	3,112	4,107	3,053	4,913
Castagna (Eq. 2.34)	7,236	5,553	2,981	3,579
Han (Eq. 2.37)	7,019	8,335	4,938	5,109

Table 5.7: Test of model derived from well 16/2-4, North Sea

Model	Average error (%)			
	On its own well Norwegian Sea	*Far wells North Sea*	*Nearby wells Norwegian Sea*	*Very far wells Barents Sea*
*This thesis (*Eq. 4.35*)*	1,405	5,179	x	3,381
Castagna (Eq. 2.34)	2,981	5,553	2,981	3,579
Han (Eq. 2.37)	4,938	8,335	4,938	5,109

Table 5.8: Test of model derived from well 6608/10-17S, Norwegian Sea

Model	Average error (%)			
	On its own well Barents Sea	*Very far wells North Sea*	*Far wells Norwegian Sea*	*Nearby wells Barents Sea*
*This thesis (*Eq. 4.41*)*	2,704	5,151	1,418	3,373
Castagna (Eq. 2.34)	2,907	5,553	2,981	3,579
Han (Eq. 2.37)	4,829	8,335	4,938	5,109

Table 5.9: Test of model derived from well 7324/7-2, Barents Sea

5.4 Multivariate density models

The multivariate regression models include two more parameters and show an improved R^2 value as compared with the single parameter based model. The prediction of the multivariate based density models compared with Gardner's and Petter's models are presented in Table 5.10 and Table 5.11. Results show a lower error rate for the multivariate regression model on its own well and nearby wells, compared with the literature models. For the very far wells Gardner's and Petter's models also show quite good prediction. However, the comparisons here is based on a single well dataset. It is important to test the model on several other wells data to make more conclusive remarks.

Model	Average error (%)		
	On its own well North Sea	*Nearby wells North Sea*	*Very far wells Barents Sea*
*This thesis (*Eq. 4.43*)*	1,071	2,427	6,211
Gardner (Eq. 2.28)	2,867	2,679	5,075
Petter (Eq. 2.30)	3,529	2,751	4,181

Table 5.10: Test of model derived from well 16/2-3, North Sea

Model	Average error (%)		
	On its own well Barents Sea	*Very far wells North Sea*	*Nearby wells Barents Sea*
*This thesis (*Eq. 4.46*)*	1,855	9,114	2,201
Gardner (Eq. 2.28)	5,452	2,679	5,213
Petter (Eq. 2.30)	4,418	2,751	6,029

Table 5.11: Test of model derived from well 7374/7-2, Barents Sea

5.5 Multivariate compressional velocity

Similarly, the multivariate compressional velocity models (Eq. 4.44 and Eq. 4.45) are tested on the three basins well data. The model prediction is compared with literature Castagna's and Han's models. Table 5.12 and Table 5.13 show the results. As provided in the tables, the same trend is observed as for the multivariate density model test result. The application of the models has a higher degree of precision for its own area where the models are developed, compared with the far field wells. However, at the far field, Castagna's (Eq. 2.34) model predictions are better than this thesis' work and Han's (Eq. 2.37) model.

Model	Average error (%)		
	On its own well North Sea	*Nearby wells North Sea*	*Very far wells Barents Sea*
*This thesis (*Eq. 4.44*)*	2,319	3,503	8,205
Castagna (Eq. 2.34)	7,022	4,888	3,553
Han (Eq. 2.37)	7,208	7,630	5,045

Table 5.12: Test of model derived from well 16/2-4, North Sea

Model	Average error (%)		
	On its own well Barents Sea	*Very far wells North Sea*	*Nearby wells Barents Sea*
*This thesis (*Eq. 4.45*)*	1,865	8,208	2,357
Castagna (Eq. 2.34)	2,913	4,888	3,553
Han (Eq. 2.37)	4,805	7,630	5,045

Table 5.13: Test of model derived from well 7324/7-2, North Sea

6 Application of models

For structural engineering design works, the physical, mechanical and elastic properties of the material are used in the simulation. Among these, the wellbore stability, well bore casing and tubing design. As reviewed in the literature study part, the wellbore fracturing and well collapse model is a function of in-situ stress, pore pressure, rock uniaxial compressive strength, tensile strength, Young's modulus, Poisson ration as well as internal friction angle are relevant. The parameters are estimated from well log datasets. In the absence of logs, the reviewed literature models and this thesis' models estimate the missing log. This section presents the estimated logs, and their application for the determination of parameters. In Appendix A1 the application of this thesis work is summarized.

6.1 Application #1: Estimation of Logs

6.1.1 Density log estimation

Figures Figure 6.1-Figure 6.4 show the estimation of density log from compressional wave velocity using Gardner' model (Eq. 2.28), Petter's model (Eq. 2.30), and the models derived in this study based on single parameter(Eq. 4.3) and multivariate(Eq. 4.43) regression models. Results show that the new model prediction is better than Gardner and Petter's models estimations. Comparing with the single parameter model, the multivariate model reduces the error percentile deviation.

Model	This Thesis **(**Eq. 4.43**)**	This Thesis **(**Eq. 4.3**)**	Gardner (Eq. 2.28)	Petter (Eq. 2.30)
Average error (%)	1,071	2,307	2,867	3,284

Table 6.1: Comparison of density log estimation

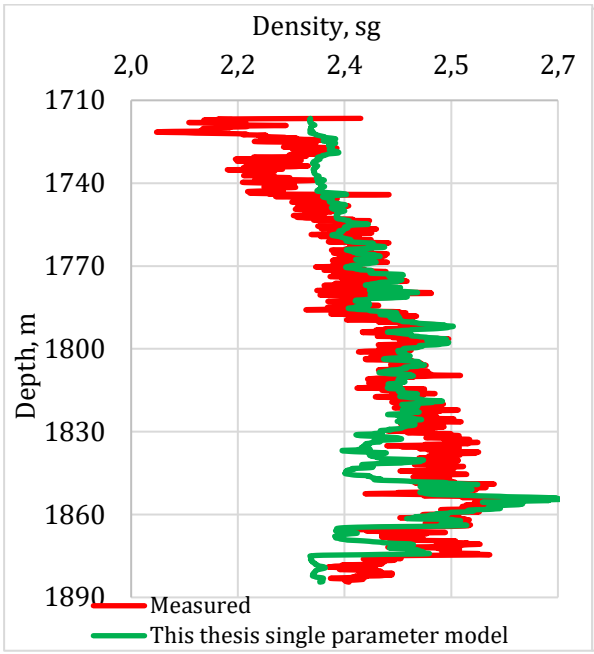

Figure 6.1: Comparison between this thesis single parameter model and measured density

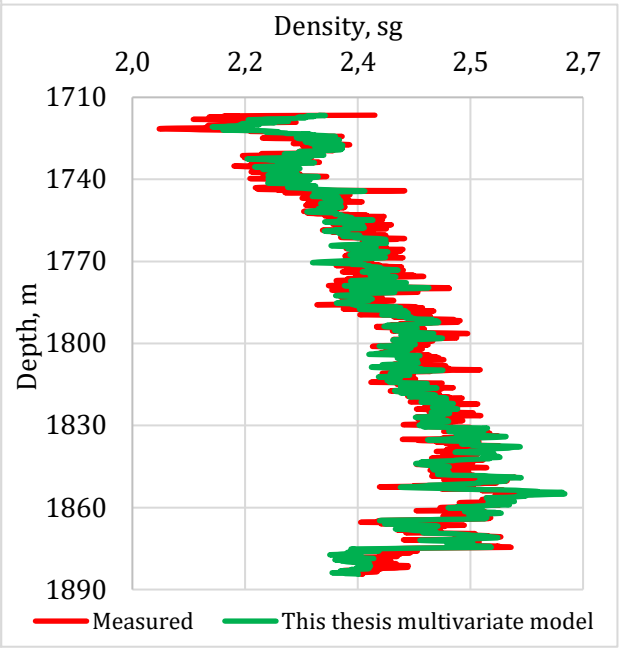

Figure 6.2: Comparison between this thesis multivariate model and measured density

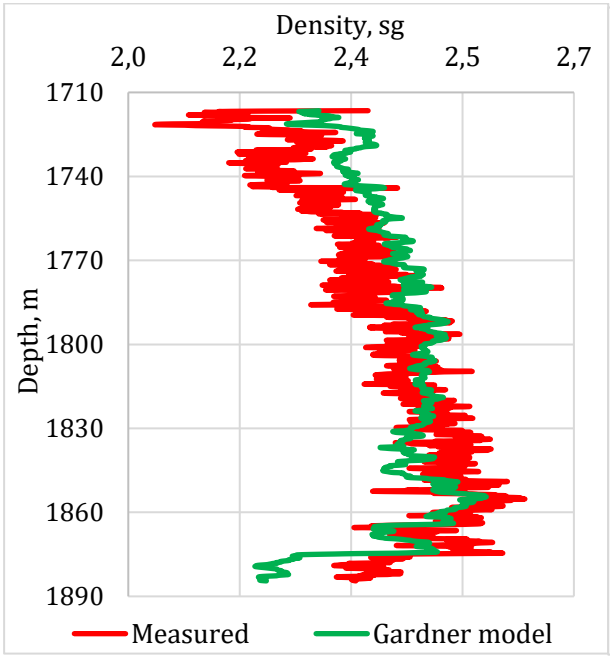

Figure 6.3: Comparison between Gardner model and measured density

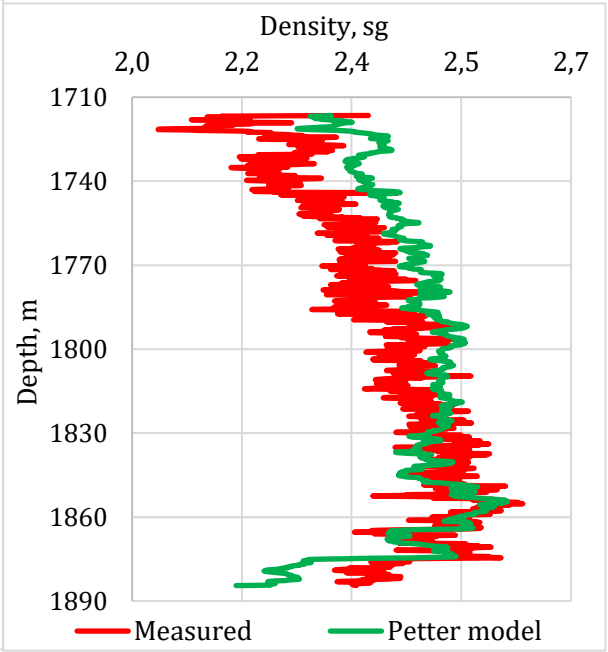

Figure 6.4: Comparison between Petter model and measured density

6.1.2 Compressional Velocity log Estimation

In this section the compressional velocity log estimated from shear velocity by using the Castagna (Eq. 2.34), Han (Eq. 2.37) and this thesis work models (i.e. single parameter Eq. 4.41 and multivariate regression models Eq. 4.45) are presented.

Results again show, in Table 6.2, that the multivariate regression model prediction reduced the error deviation compared with the literature models. Moreover, the single parameter-based prediction is better than Castagna's model and Han's model as well.

Model	This Thesis (Eq. 4.45)	This Thesis (Eq. 4.41)	Castagna (Eq. 2.34)	Han (Eq. 2.37)
Average Error (%)	1,865	2,702	2,913	4,805

Table 6.2: Comparison of Velocity log estimation

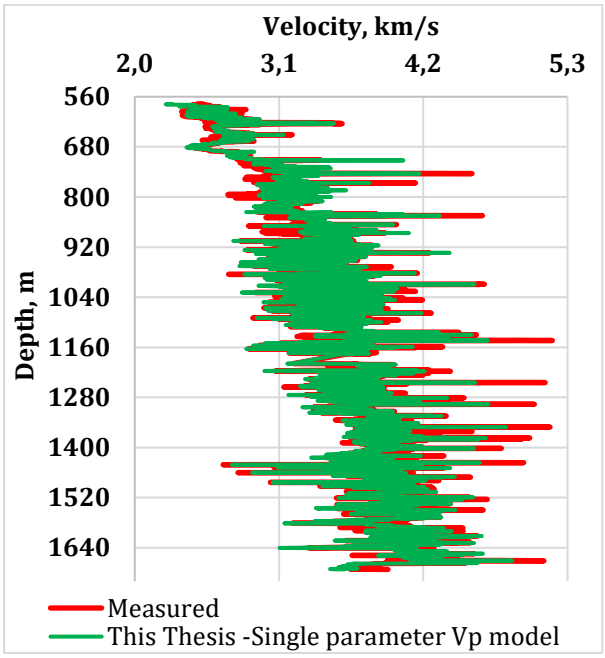

Figure 6.5: Comparison between this thesis single parameter model and measured density

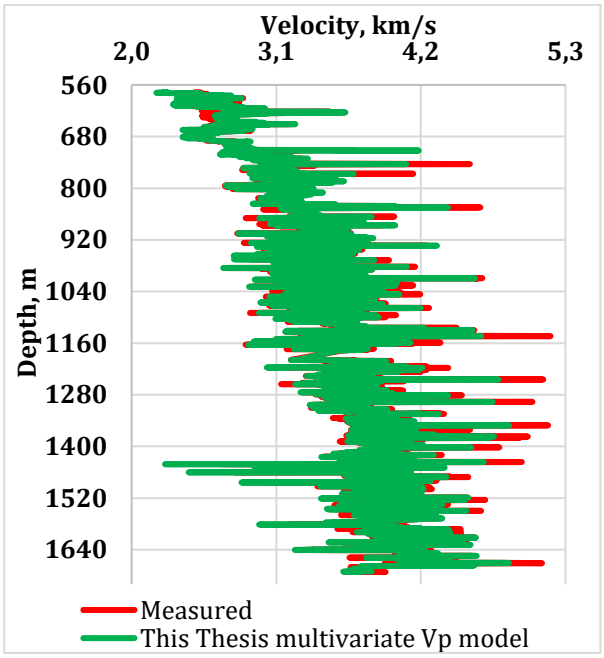

Figure 6.6: Comparison between this thesis multivariate model and measured density

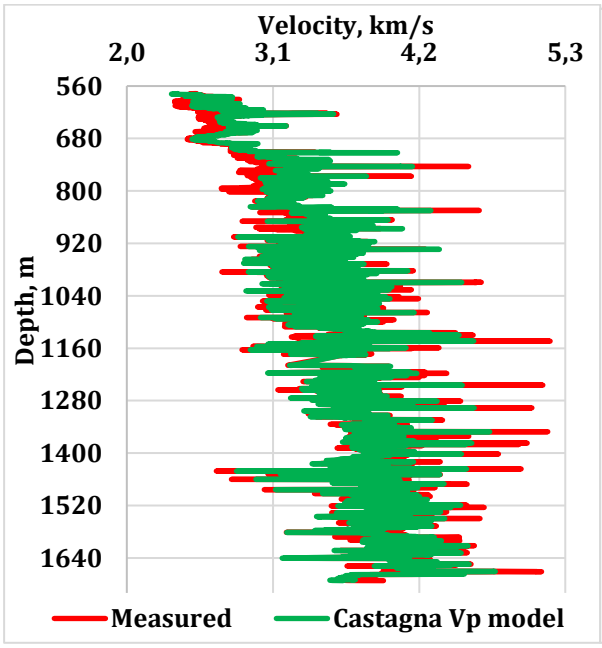

Figure 6.7: Comparison between Castagna model and measured compressional velocity

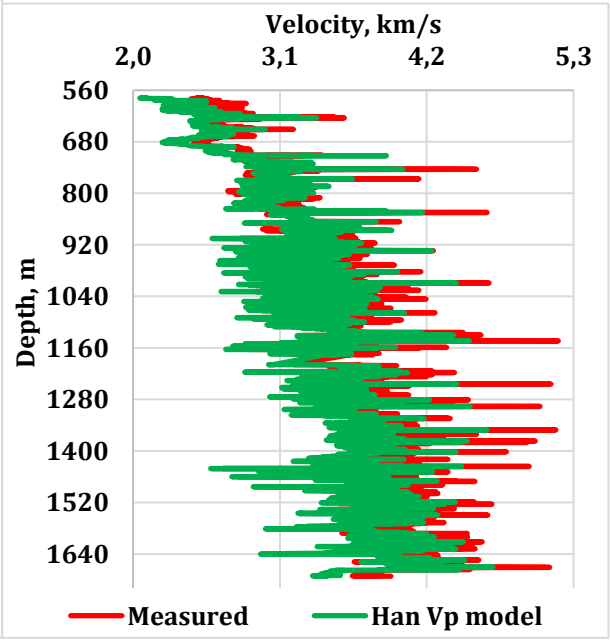

Figure 6.8: Comparison between Han model and measured compressional velocity

6.2 Application #2: Geophysics -Acoustic impedance and reflection coefficient

Geophysicists generate synthetic trace in order to correlate with measured seismic trace reflectors. For this, the reflectivity and acoustic impedance ($AI=\rho V_p$) are calculated from the product of the measured compressional sonic and density. The AI describe the formation properties. In the absence of density log, the density is estimated from Gardner's density-velocity empirical model. Similarly, the compressional wave velocity is estimated from Castagna's model, when the velocity log is missing. These are popular empirical models. However, the performance of these models will be compared with models derived in this thesis work, and Petter's model that has been developed from Norwegian continental shelf data. The reflective coefficient is calculated from the acoustic impedance of the top and the bottom layer: (Rider & Kennedy, 2018)

$$R = \frac{\rho_2 V_2 - \rho_1 V_1}{\rho_2 V_2 + \rho_1 V_1} = \frac{AI_2 - AI_1}{AI_2 + AI_1} \qquad \text{Eq. 6.1}$$

As shown in Eq. 6.1, the acoustic impedances were calculated from the measured density and velocity logs. Assuming that only the velocity log is available (North Sea well 16-2-3 data), the density log is estimated from literature empirical models (Gardner model Eq. 2.28 and Petter model Eq. 2.30). Density log also estimated from the newly derived density models, which are based on a single parameter model (Eq. 4.3) and a multivariate regression model (Eq. 4.43). Then using the acoustic impedances, the reflection coefficient is calculated. Figure 6.9, Figure 6.10, Figure 6.11 and Figure 6.12 show the comparisons between the density and velocity measured reflection coefficient with measured velocity log and the model derived density log.

As shown in the figures, the multivariate regression model based reflection coefficient prediction is better than the single parameter model based predictions (like Gardner's and Petter's density inverted models). However, the literature models also predict quite well.

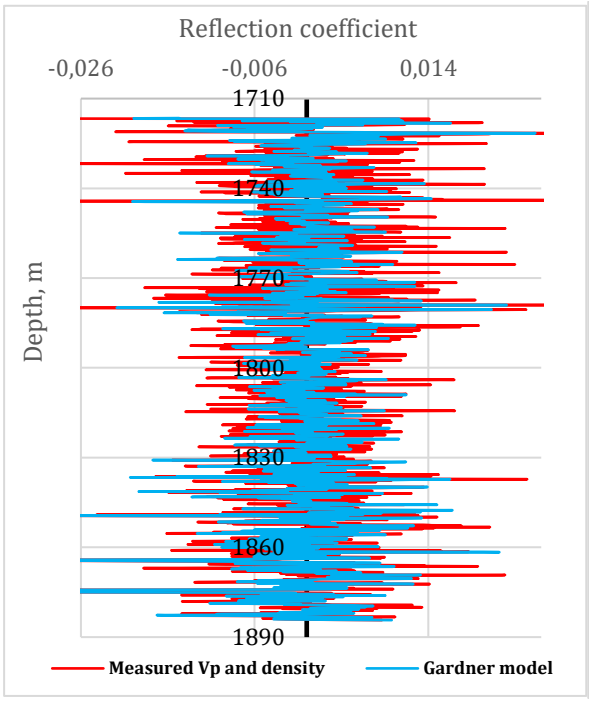

Figure 6.9: Reflection coefficient prediction from the inverted Gardner density model and the measured compressional wave velocity compared with the measured density and compressional wave velocity logs.

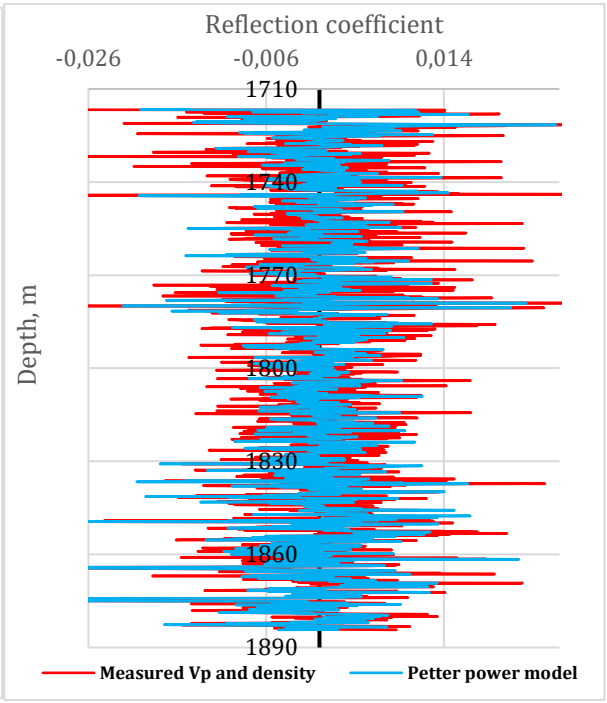

Figure 6.10: Reflection coefficient prediction from the inverted Petter density model and the measured compressional wave velocity compared with the measured density and compressional wave velocity logs.

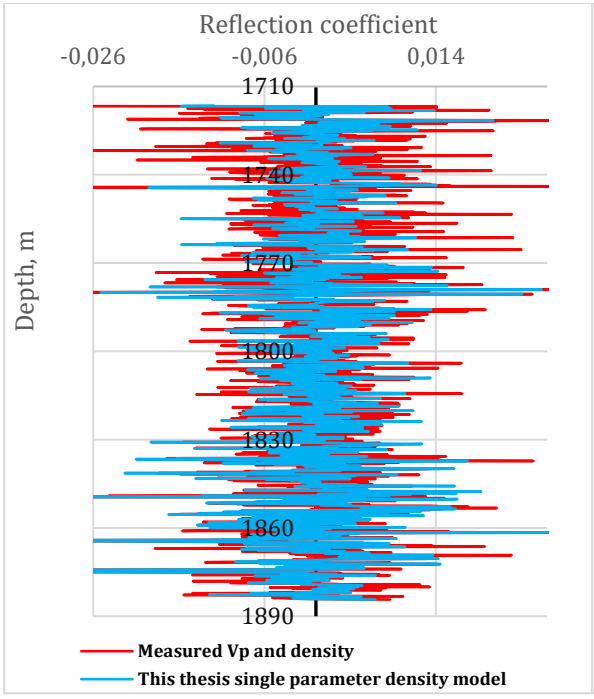

Figure 6.11: Reflection coefficient prediction from the inverted this thesis single parameter density model and the measured compressional wave velocity compared with the measured density and compressional wave velocity logs.

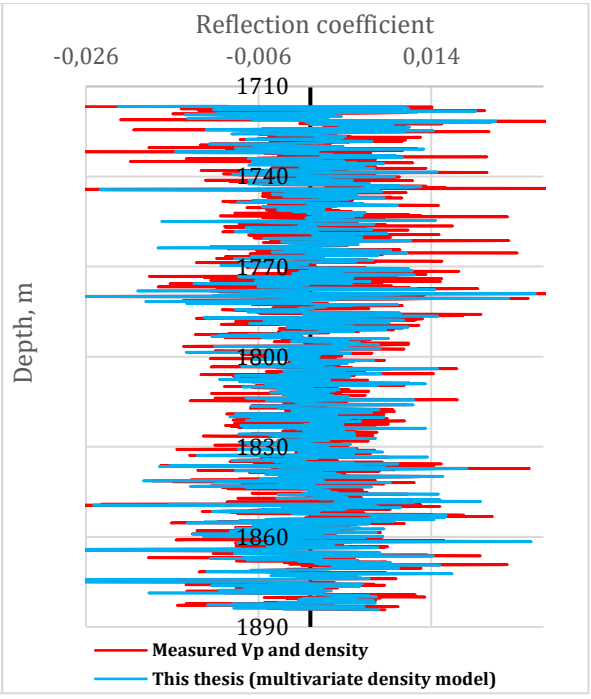

Figure 6.12: Reflection coefficient prediction from the inverted this thesis multivariate regression density model and the measured compressional wave velocity compared with the measured density and compressional wave velocity logs.

6.3 Application #3: Geomechanics/well stability and ROP modelling

As reviewed in the literature study part (section 2.2), the wellbore fracturing and well collapse models are a function of in-situ stress, pore pressure, rock uniaxial compressive strength, tensile strength, Poisson ratio, and Young' modulus parameters.

The Mechanical specific energy MSE describe the amount of energy required to excavate a unit volume of rock. The MSE is a parameter for the Rate of penetration determination. However, when drilling a new well, the MSE value can be estimated with the Uniaxial compressive strength of the rock. MSE can be related with the UCS as: (Hammoutene, 2012)

$$\frac{UCS}{MSE} = EFE_M \qquad \text{Eq. 6.2}$$

Where, EFF_M is mechanical bit efficiency of 0,3-0,64.

6.3.1 UCS prediction

UCS is an essential parameter for the Well collapse and ROP modelling. Therefore, the Horsrud (Horsrud, 2001)(Eq. 2.21) model is used to determine UCS, this empirical model is a function of compressional velocity. However, in the absence of compressional velocity, this study's models or the literature models can be utilized. In the following figures these models are applied and compared with the log based UCS calculation. Figure 6.16, as well as Table 6.3, show that the multivariate model is superior.

Model	This Thesis (Eq. 4.45)	This Thesis (Eq. 4.41)	Castagna model (Eq. 2.34)	Han model (Eq. 2.37)
Average error (%)	5,480	8,012	8,825	13,323

Table 6.3: Comparison of UCS predictions

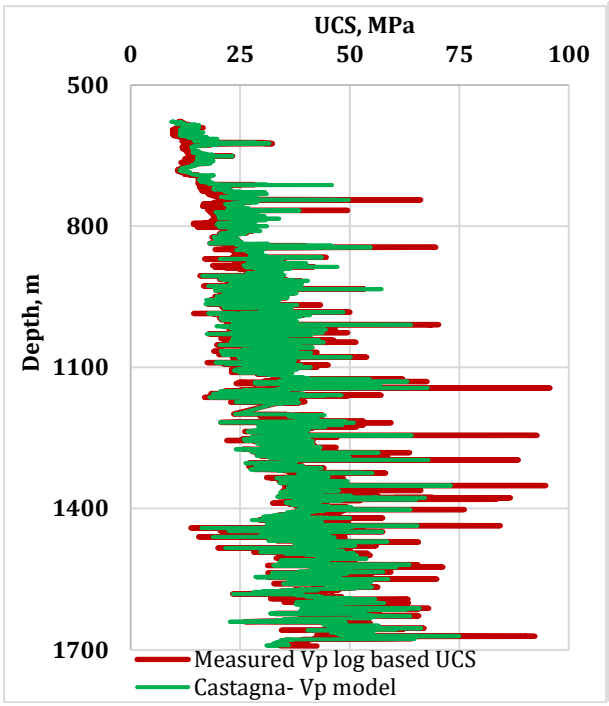

Figure 6.13: Prediction of UCS from the compressional wave velocity inverted from shear wave velocity using Castagna model and from the measured compressional velocity log data

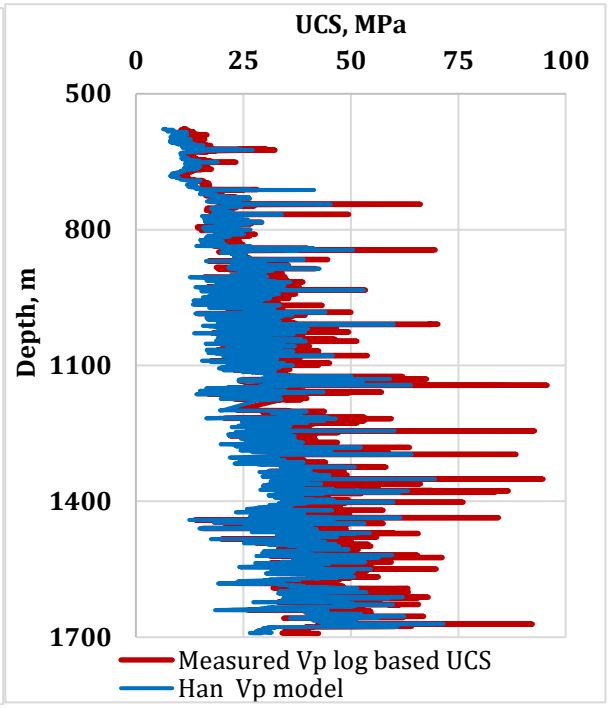

Figure 6.14: Prediction of UCS from the compressional wave velocity estimated shear wave velocity using Han model and from the measured compressional velocity log data

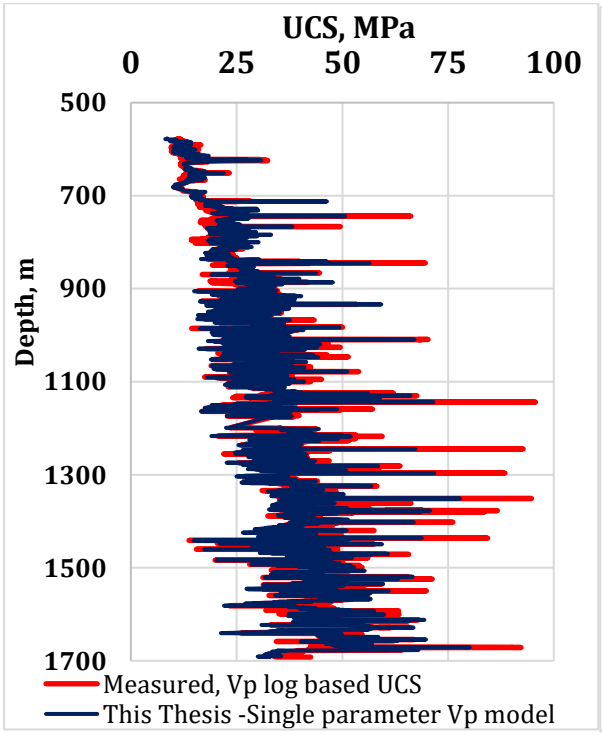

Figure 6.15: Prediction of UCS from the compressional wave velocity estimated from thhis thesis single parameter shear wave velocity model and from the measured compressional velocity log data

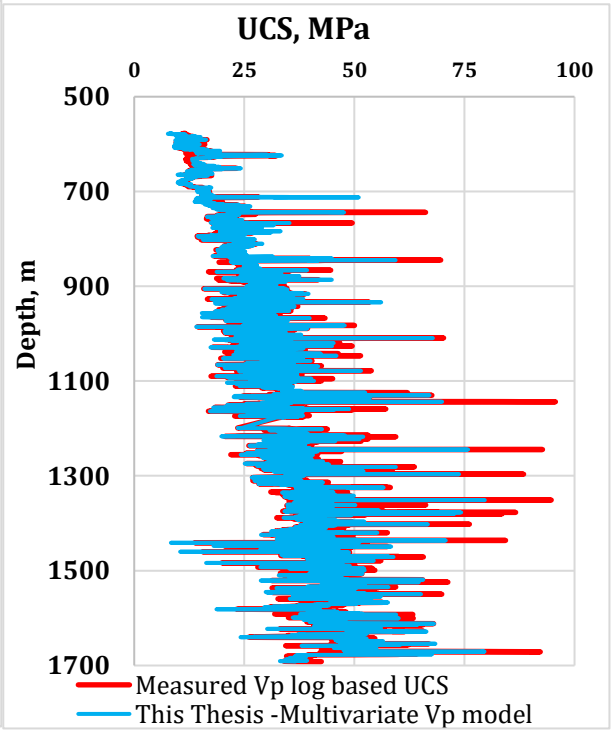

Figure 6.16: Prediction of UCS from the compressional wave velocity estimated from this thesis multivaraite regression model and from the measured compressional velocity log data

6.3.2 E-modulus predictions

Like the UCS, the Horsrud model (Eq. 2.21) is used to estimate the E-modulus of the drilling formation. The E-modulus is predicted based on the compressional velocity. The compressional wave velocities were estimated from literature models (Castagna Eq. 2.34 and Han Eq. 2.37) and the new models (i.e. Single parameter model Eq. 4.41 and multivariate regression model Eq. 4.45).

Model	This Thesis (Eq. 4.45)	This Thesis (Eq. 4.41)	Castagna model (Eq. 2.34)	Han model (Eq. 2.37)
Average error (%)	6,033	8,844	9,761	14,537

Table 6.4: Comparison of E-modulus predictions

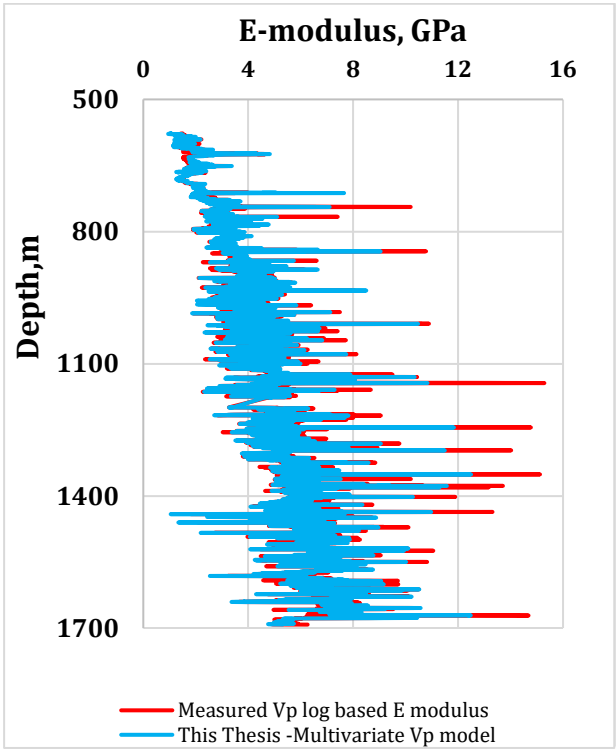

Figure 6.17: E-modulus prediction from compressional velocity inverted from this thsis single parameter model and measured compressional velocity log data

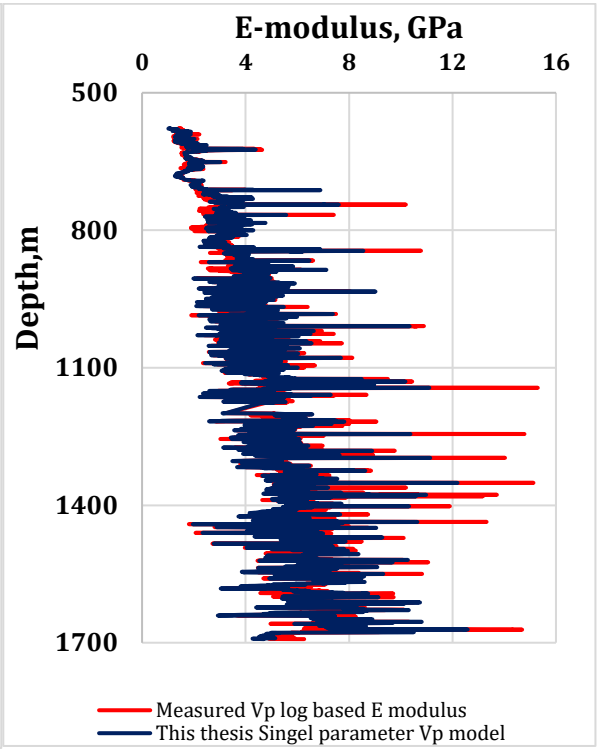

Figure 6.18: E-modulus prediction from compressional velocity inverted from this thesis multivatrate model and measured compressional velocity log data

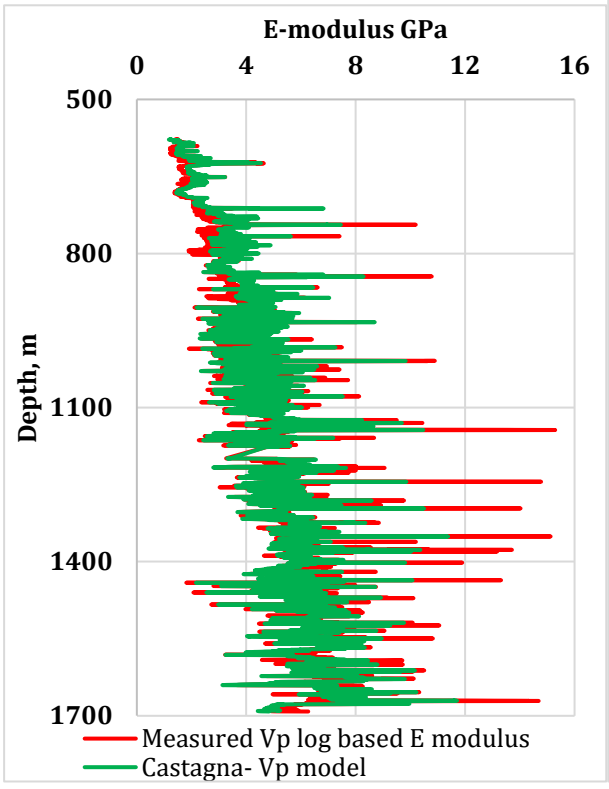

Figure 6.19: E-modulus prediction from compressional velocity inverted from Castagna model and measured compressional velocity log data

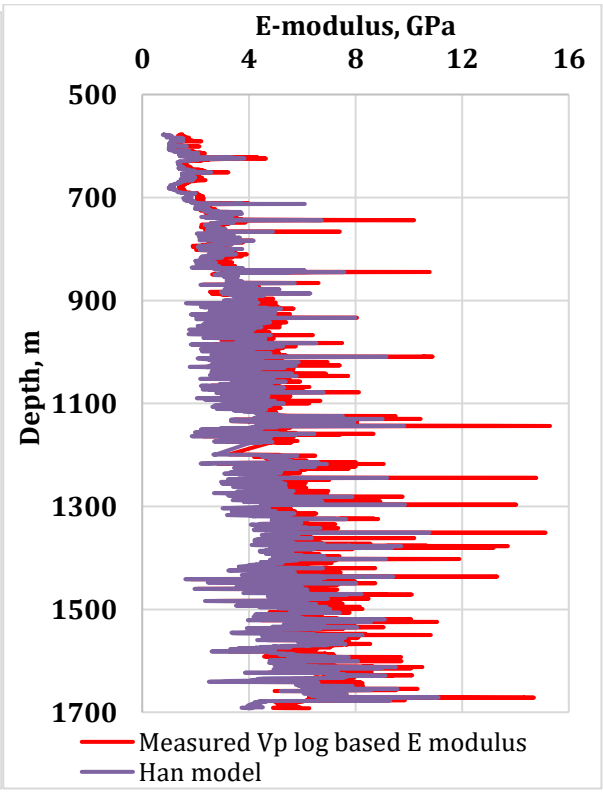

Figure 6.20: E-modulus prediction from compressional velocity inverted from Han model and measured compressional velocity log data

6.3.3 Poisson's ratio predictions

The Poisson's ratio is normally determined from compressional and shear velocity. In this example, assuming that only the shear velocity log data is available, the compressional velocity will be estimated from Castagna model (Eq. 2.34) and this thesis multivariate model (Eq. 4.45). Figure 6.21 and Figure 6.22 show the Poisson's ratio derived from the measured dataset compared with the compressional velocity estimated log based ratio. Results show that the multivariate based Poisson's ratio record the average percentage error of 3.832% and the Castagna model based recorded 5.821% error deviations.

Model	This thesis (Eq. 4.45)	Castagna (Eq. 2.34)
Average error (%)	3,832	5,821

Table 6.5: Comparison of Poisson's ratio predictions

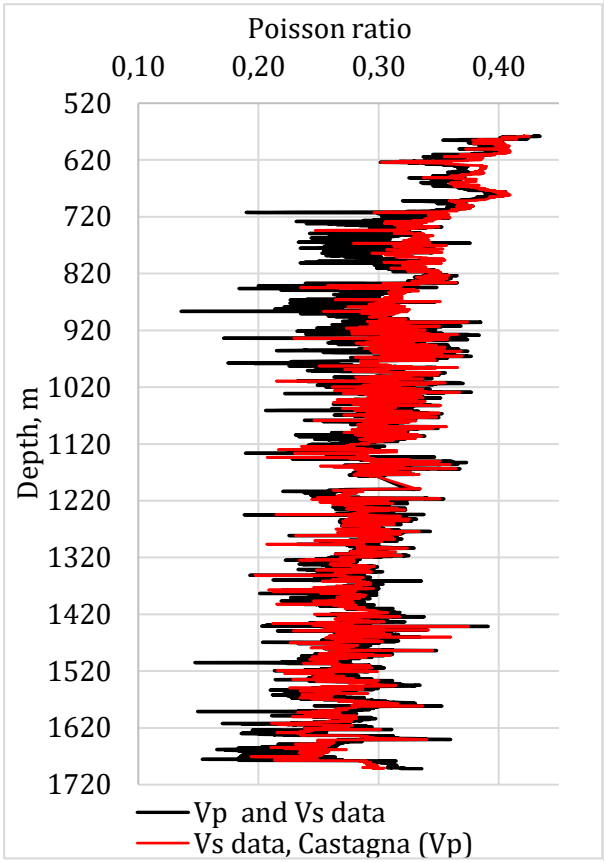

Figure 6.21: Comparisons of Poisson ratio estimation from compressional velocity estimated by using Castagna model and measured shear velicity with the measured compressional and shear velocity log data

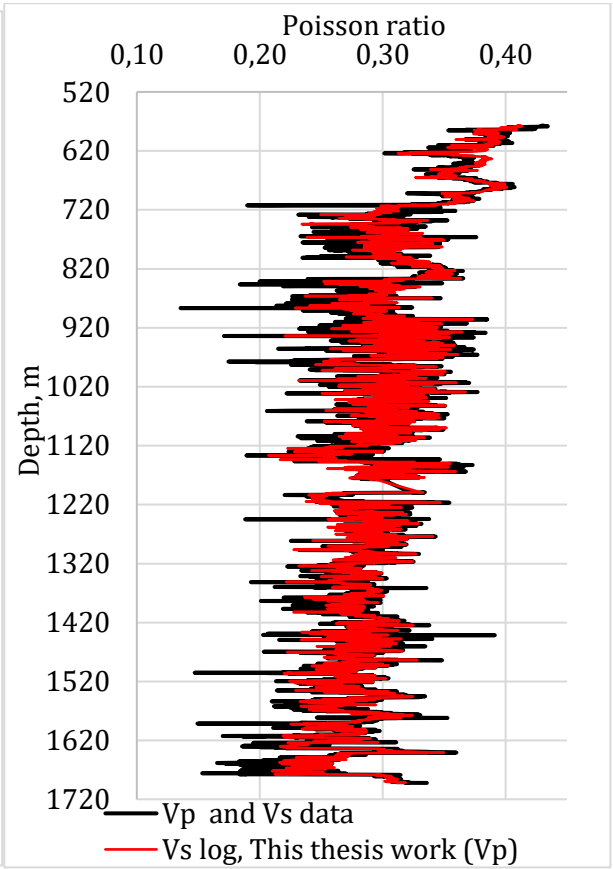

Figure 6.22: Comparisons of Poisson ratio estimation from compressional velocity estimated by using this thesis multivatate regression model and measured shear velicity with the measured compressional and shear velocity log data

7 Artificial Neural Network Method Modelling

An artificial neural network (ANN) also known as neutron network is the process of computing system that simulates in similar manner as biological neural networks_operates in human brain capable of learning, prediction and recognition (Agatonovic-Kustrin & Beresford, 2000). Machine learning is a branch of artificial intelligence, which encompasses several fields of studies such as, computer science, mathematics and computational statistics.

As illustrated in Figure 7.1, an ANN is designed with artificial neurons, which are processing units having coefficients (weights). The neural structures are organized in layers as input layer, the hidden layer and the output layer.

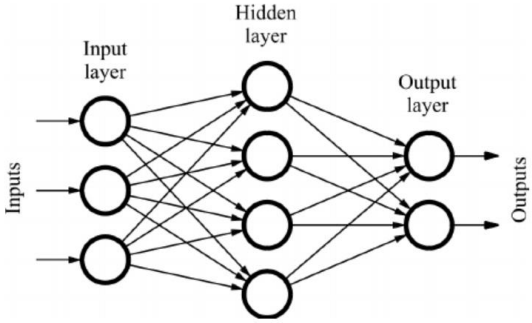

Figure 7.1: Feedforward Artificial new works (ANN) architecture (Agatonovic-Kustrin & Beresford, 2000)

The artificial neurons have weighted inputs, transfer function, and the target output. The activation of the neuron uses the weighed sum of the inputs. As illustrated in Figure 7.2, the single output of the neuron is generated after passing the activation signal through transfer function.

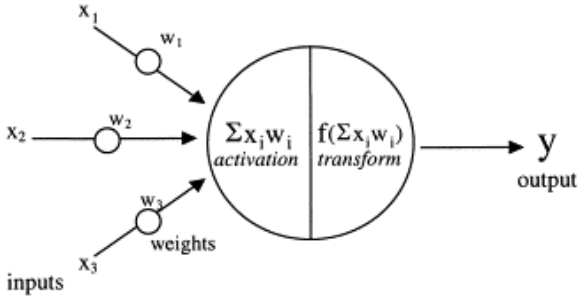

Figure 7.2: Model of an artificial neuron(Agatonovic-Kustrin & Beresford, 2000).

7.1 Single input and density modelling

To compare the single parameter-based regression model, machine learning data driven based modelling technique is implemented. The density of the drilling formation was modelled by using a Feed-forward back propagation network. The training algorithm used in this study was the **Levenberg–Marquardt** algorithm (TRAINLM). The network training function updates weight and bias values. In addition, the LEARNGDM adaptation learning function is used to calculate the change weight and update returns the weight change and a new learning state. Figure 7.3 shows the network properties used for the modeling (Mathworks, 2021b):

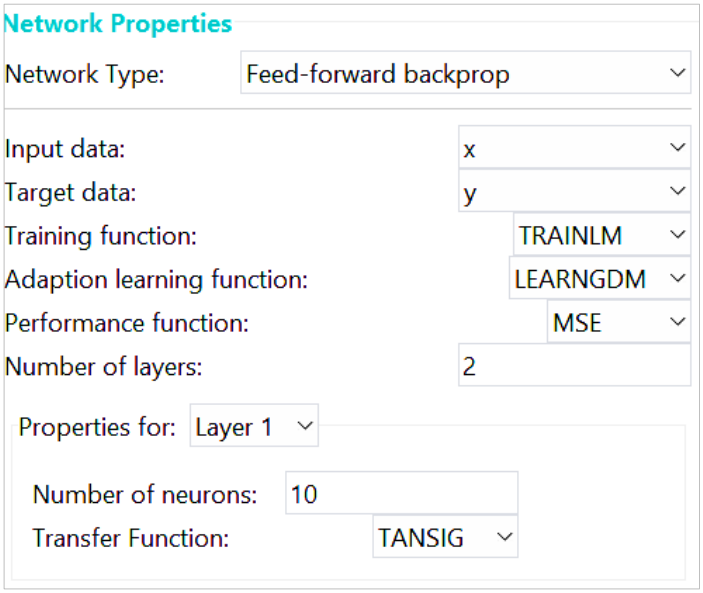

Figure 7.3: Types of Artificial Neural Networks – FeedBack ANN (Mathworks, 2021b)

The network was built with three layers, input layer, hidden layer and output layer. The input layer consists of one neuron (i.e. Velocity), the hidden layer are 10 neurons and TANSIG transfer function, and the output layer has one neuron (i.e. Density) and the sigmoid TANSIG transfer function. In Figure 7.4 the input is velocity and the target is density.

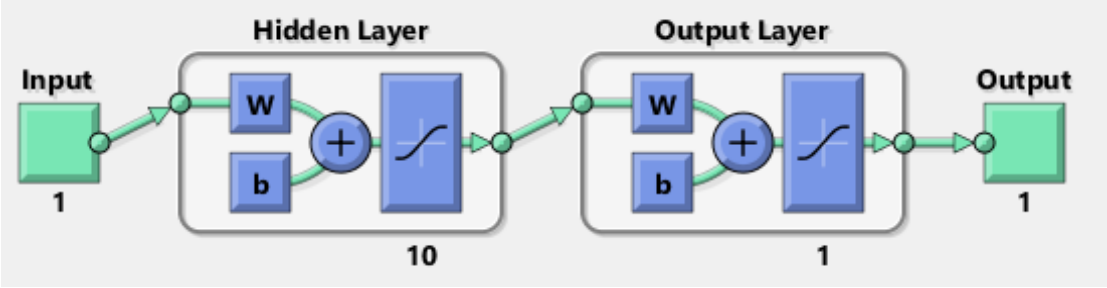

Figure 7.4: Network for single input parameter-based modelling(Mathworks, 2021a)

Mathematically, the model in terms of weight and bias for density prediction

$$\rho = \left\{ \sum_{i=1}^{N} W_{2i} TANSIG \left(\sum_{j=1}^{J} W_{2i} \times X_j + b_{1i} \right) \right\} + b_2 \qquad \text{Eq. 7.1}$$

Where,

- *N* is the number of neurons which was optimized to be 10 for the hidden layer,
- *W2i* is weight of the output layer,
- *J* is the number of input variables,
- *W1* is weight of hidden layer,
- *Xj* is the input variable (Vp),
- *b1* is bias of the hidden layer, and
- *b2* is bias of the output layer.

ANN model was developed using velocity as inputs to predict density. MATLAB program divided the dataset into ratios of 70 percent for training and 30 percent for testing.

Figure 7.5 shows a quite good match between the predicted and the measured density with R-value of 0.84591 for the training process and 0.86481 for the testing process.

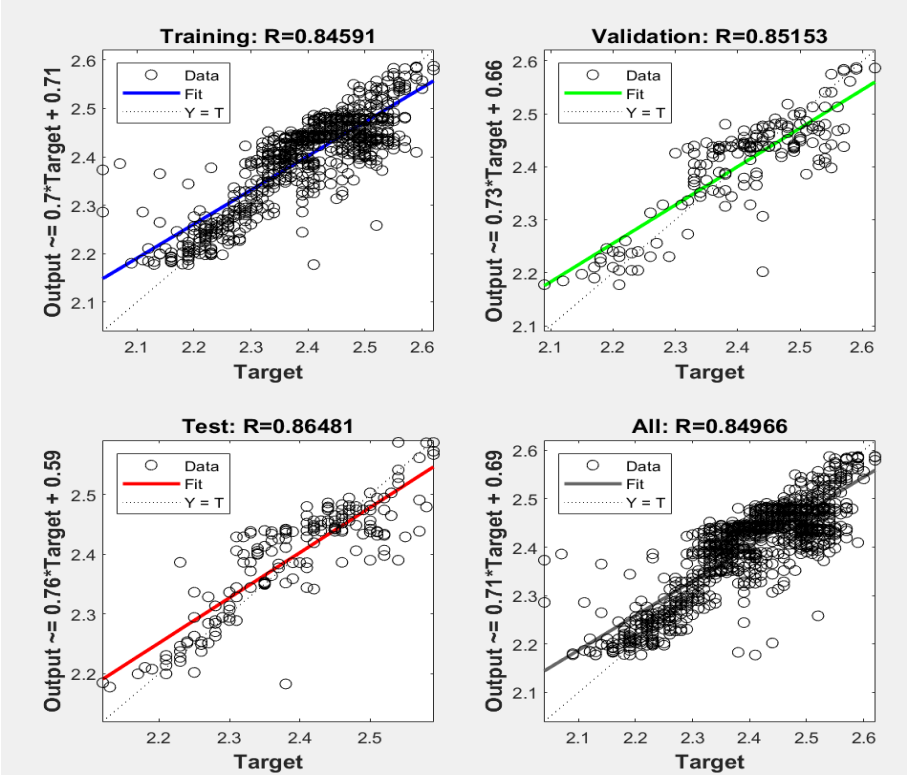

Figure 7.5: ANN model training, testing and validation output of single input parameter modelling results

Figure 7.7 shows the comparison between the ANN and the measured data. Similarly, Figure 7.6 displays the comparison between this thesis single parameter-based regression models prediction with the measured data. For a better comparison, the calculated average percentile deviation between the single parameter regression model and single parameter ANN model prediction measurements are shown in Figure 7.8.

Results show that the ANN model reduced the error rate by 22.4% as compared with the regression model. The main reason is that the regression model is a single run, but the ANN model feed the errors until an optimized improved fitting is achieved.

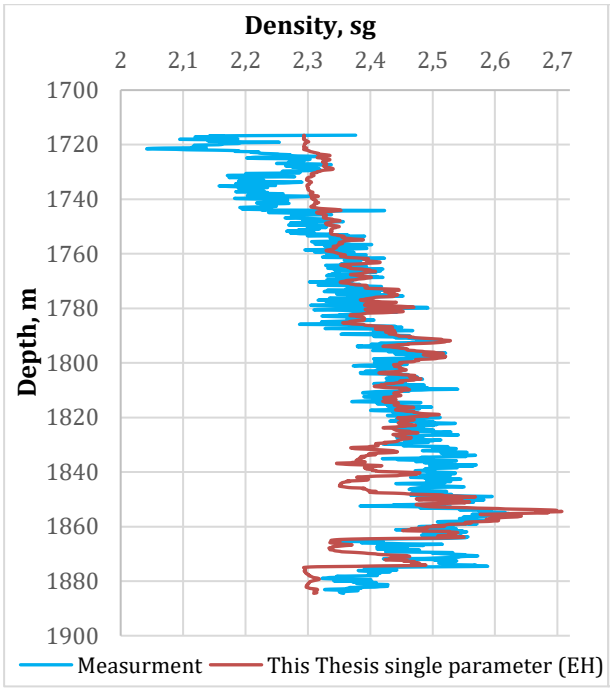

Figure 7.6: Comparison between this thesis single compressional velocity model and and measured density log data in North Sea well (16/2-3) Eq. 4.3

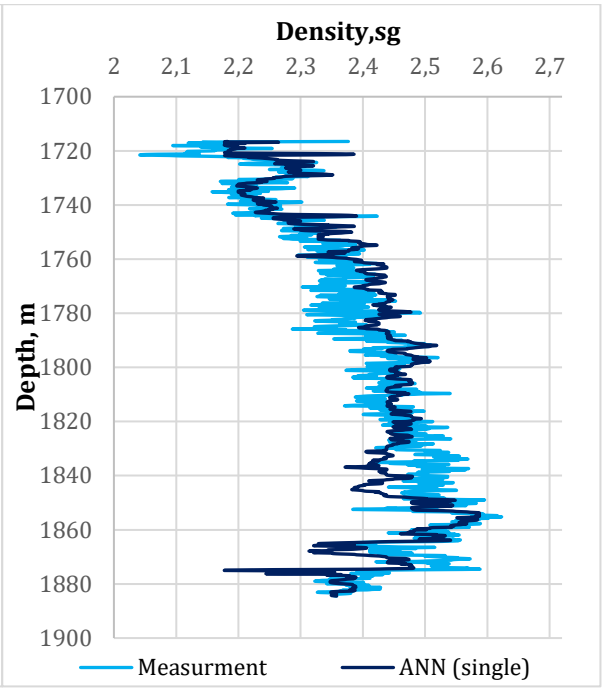

Figure 7.7: Comparison between ANN (Single parameter input) and measured density log data obtatined fron North Sea well (16/2-3)

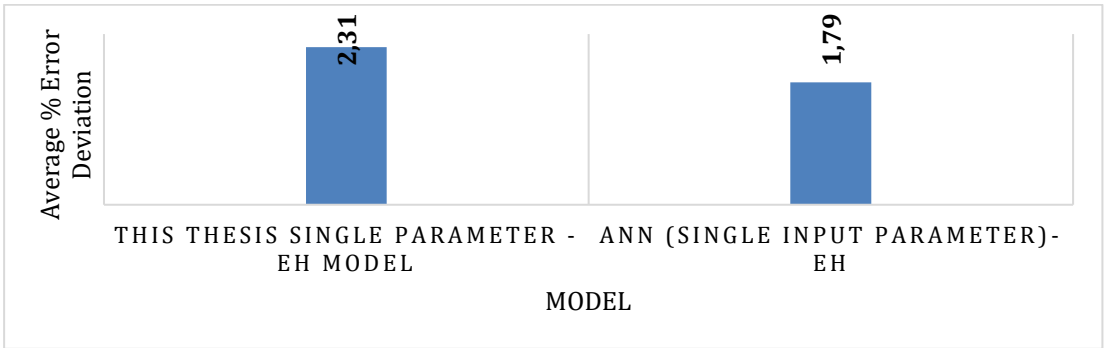

Figure 7.8: The average % error deviation of this thesis works single parameter model (EH-Eline and Haakon Eq. 4.3) and ANN single parameter input model predictions from the measurement.

7.2 Multiple inputs and density modelling

The modelling approach is like the previous section with the feed-forward back propagation network. The training algorithm and the adaptation functions are (TRAINLM) and LEARNGDM respectively. As shown in Figure 7.9, the network was built with 3 layers, input layer, hidden layer and output layer. The input layer consists of 3 neuron (compressional velocity, shear velocity and Porosity), the hidden layer are 10 neurons and TANSIG transfer function, and the output layer has 1 neuron (Density) and TANSIG transfer function.

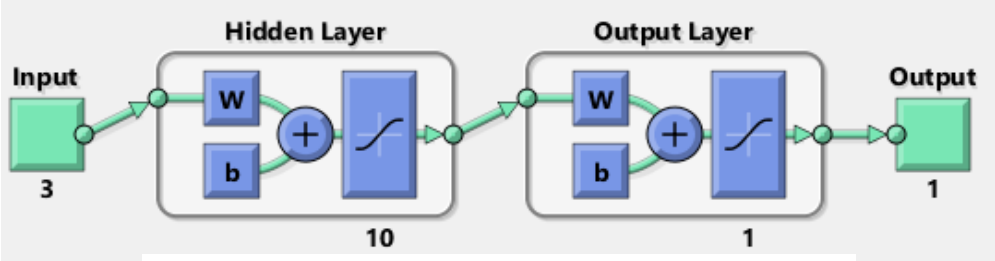

Figure 7.9: Network for three input parameters-based modelling (Mathworks, 2021a)

Figure 7.10 show an improved match between the predicted and the measured density with R-value of 0.97221 for the training process and 0.96781 for the testing process.

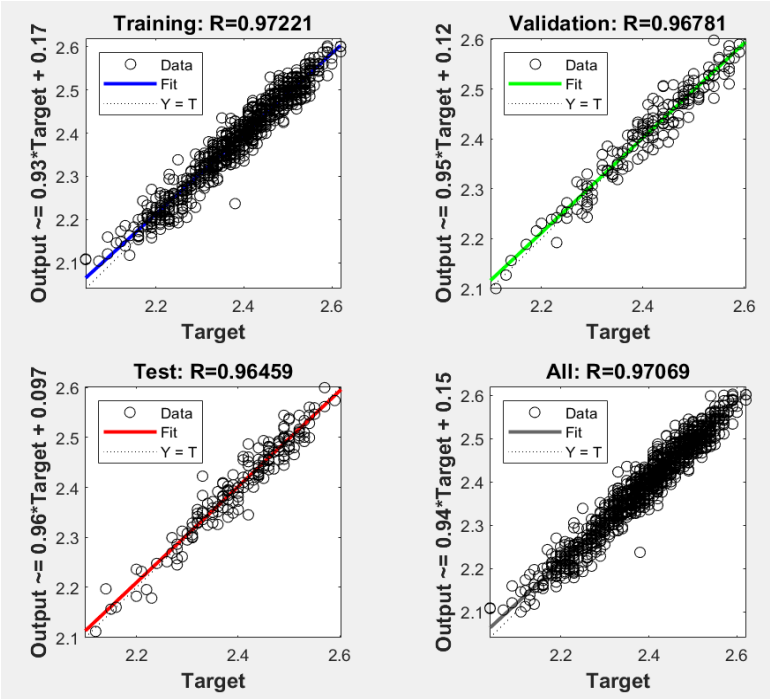

Figure 7.10: ANN model training, testing and validation output of three input parameters modelling results

Figure 7.12 shows the comparisons between the ANN and the measured data. Figure 7.11 also displays the comparisons between this thesis multivariate based regression model prediction with the measured data. As shown in Figure 7.13, the calculated average error percentile deviation between the multivariate regression model and the measurements records is 1.07 % and the ANN model records 0.84%. Comparing these, the ANN model reduced the error rate by 21.5% as compared with the regression model.

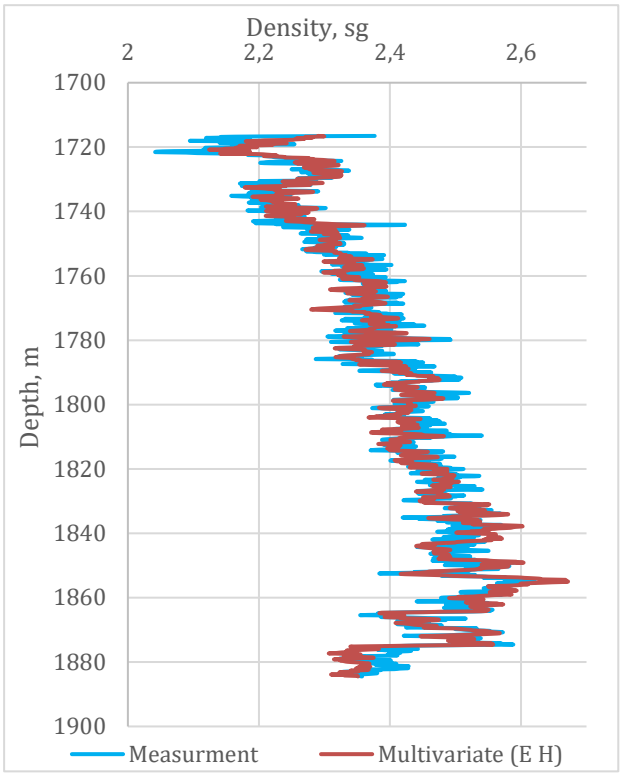

Figure 7.12: Comparison between this thesis multivarate regression density model and measured density log data in the North Sea well 16/2-3 (Eq. 4.43)

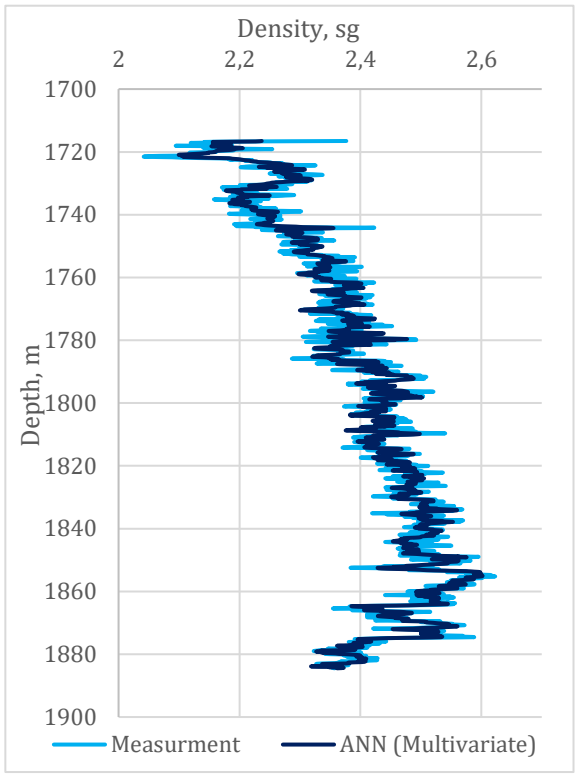

Figure 7.11: Comparison between ANN (three input parameters) and measured density log data in North Sea well 16/2-3

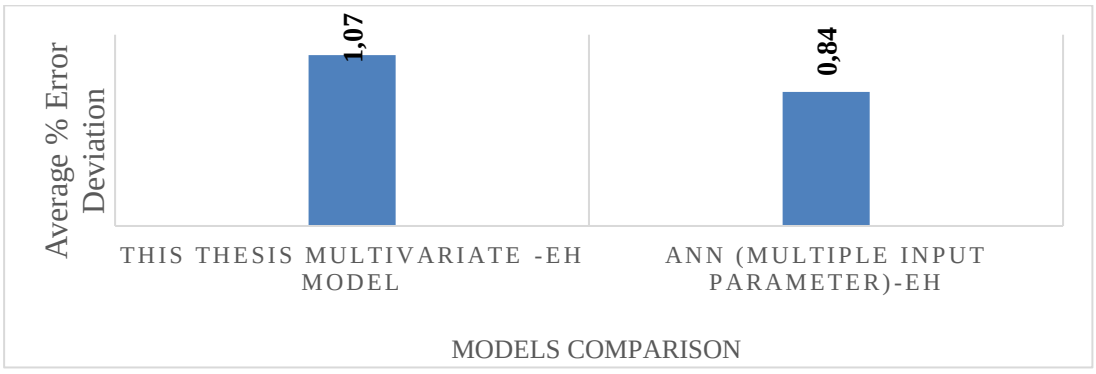

Figure 7.13: The average % error deviation of this thesis work multivariate regression model (EH-Eline and Haakon Eq. 4.43) and ANN three input parameters model predictions from the measurement

8 Uncertainty

- Visualizing and preprocessing is essential, this include removal of unrecorded datasets and outliers. Otherwise the model prediction would be poor.
- The quality of the dataset with regards to environmental correction of the log dataset would improve the modelling result. However, due to insufficient information and unviability of environmental correction charts, this may increase uncertainty regarding the quality of the data.
- The modelling results obtained from the Barents Sea wells, show relatively poor correlation for models involving density. This surely is related to the quality of the dataset, and might be associated with the measuring tools, or the lack of environmental correction data.

9 Conclusion

In this thesis, several wells' data from the Barents Sea, Norwegian Sea and North Sea were used to model density and velocity. The modelling was based on single and multivariate regression methods. Moreover, artificial neuron network (ANN) modelling technique is implemented. The performance of the developed model was evaluated by comparing with the commonly used literature models, which are developed from fields and experimental data other than the Norwegian continental shelf. The main objectives were to evaluate the applicability of the literature models for the NCS and to develop an alternative model that will be used for the Norwegian continental shelf.

All the models developed during this thesis is presented in Appendix A 2. The models with the lowest total average error percentage are summarized in Appendix A 3. The application of the models for parameters determination are also listed in Appendix A 1.

The modelling, testing and application analysis results are summarized as:

- Multivariate density and velocity models improved the single parameter model, which reduces the percentile error deviation and increase the correlation factor R^2 value.
- Gardener's and Castagna's models work quite well. However, the local models derived in this thesis show a lower error rate.
- The application of models derived from the North Sea/Norwegian Sea/Barents Sea work well when applied in the nearby wells. The results are quite good compared to the literature models. At the very far fields, average error increase.
- ANN based modelling provided good results. Like the regression models, the ANN based on multivariate input parameters results in a good match provided that the input parameters have good correlation.

10 Future work

For future work, authors propose:

- Results showed that the multivariate regression improved the prediction compared with the single parameter. Therefore, we propose to investigate if there are more parameters that could have potential to be a part of the multivariate regression models.
- Results from the single well data have shown good performance. In order for the dataset to be more representative for the region, we propose to merge all the wells' datasets within the block and generate a model. The model will then be tested on each individual well, far and very far fields in order to investigate their application and limitation.
- Close by Sea wells dataset (e.g. North Sea with Norwegian Sea or Norwegian Sea with Barents Sea) can be merged in order to develop models.
- The possibility of including ANN modelling as shown in this thesis, can be further investigated.

11 Reference

Agatonovic-Kustrin, S., & Beresford, R. (2000). Basic concepts of artificial neural network (ANN) modeling and its application in pharmaceutical research. *Journal of pharmaceutical and biomedical analysis, 22*(5), 717-727.

Alger, R., Locke, S., Nagel, W., & Sherman, H. (1972). The dual-spacing neutron log-CNL. *Journal of Petroleum Technology, 24*(09), 1,073-071,083.

Anbazhagan, P., Uday, A., Moustafa, S. S., & Al-Arifi, N. S. (2016). Correlation of densities with shear wave velocities and SPT N values. *Journal of Geophysics and Engineering, 13*(3), 320-341.

Castagna, J. P., Batzle, M. L., & Eastwood, R. L. (1985). Relationships between compressional-wave and shear-wave velocities in clastic silicate rocks. *geophysics, 50*(4), 571-581.

Eaton, B., Bower Jr, A., & Martis, J. (1975). Manufactured Diamond Cutters Used in Drilling Bits. *Journal of Petroleum Technology, 27*(05), 552-554.

Fjar, E., Holt, R. M., Raaen, A., & Horsrud, P. (2008). *Petroleum related rock mechanics*. Elsevier.

Gardner, G., Gardner, L., & Gregory, A. (1974). Formation velocity and density—The diagnostic basics for stratigraphic traps. *Geophysics, 39*(6), 770-780.

Glover, P. (2000). Petrophysics. *University of Aberdeen, UK*.

Hammoutene, C. (2012). FEA Modelled MSE/UCS Values Optimise PDC Design for Entire Hole Section. North Africa Technical Conference and Exhibition,

Han, D.-h., Nur, A., & Morgan, D. (1986). Effects of porosity and clay content on wave velocities in sandstones. *Geophysics, 51*(11), 2093-2107.

Havnen, P. (2020). *Development of New Density-Velocity model based on NCS well field data and comparisons*
with literature models University of Stavanger].

Horsrud, P. (2001). Estimating mechanical properties of shale from empirical correlations. *SPE Drilling & Completion, 16*(02), 68-73.

image. (2020). *Area status of the Norwegian continental shelf september 2020* [Image]. https://www.norskpetroleum.no/en/exploration/licensing-position-for-the-norwegian-continental-shelf/

Karimi, M., Adelzadeh, M., & Mohammadypour, M. (2014). Formula of definite point overburden pressure of reservoir layers. *Egyptian Journal of Petroleum, 23*(2), 175-182.

Labuz, J. F., & Zang, A. (2012). Mohr–Coulomb failure criterion. In *The ISRM Suggested Methods for Rock Characterization, Testing and Monitoring: 2007-2014* (pp. 227-231). Springer.

Lal, M. (1999). Shale stability: drilling fluid interaction and shale strength. SPE Asia Pacific Oil and Gas Conference and Exhibition,

Manshad, A. K., Jalalifar, H., & Aslannejad, M. (2014). Analysis of vertical, horizontal and deviated wellbores stability by analytical and numerical methods. *Journal of Petroleum Exploration and Production Technology, 4*(4), 359-369.

Mathworks. (2021a). *Design Time Series NARX Feedback Neural Networks*. 1994-2021 The MathWorks, Inc. https://ch.mathworks.com/help/deeplearning/ug/design-time-series-narx-feedback-neural-networks.html

Mathworks. (2021b). *Types of Artificial Neural Networks – FeedBack ANN* 1994-2021 The MathWorks, Inc.

Mcdonald, J. H. (2015, July 20.). *Correlation and Linear Regression*. Sparky House Publishing. http://www.biostathandbook.com/linearregression.html

Nakoulima, O., Zahibo, N., Pelinovsky, E., Talipova, T., Slunyaev, A., & Kurkin, A. (2004). Analytical and numerical studies of the variable-coefficient Gardner equation. *Applied mathematics and computation, 152*(2), 449-471.

Nave, R. (2021). *Compton Scattering* [Image]. http://hyperphysics.phy-astr.gsu.edu/hbase/quantum/comptint.html

Rehm, B., Schubert, J., Haghshenas, A., Paknejad, A. S., & Hughes, J. (2013). *Managed pressure drilling*. Elsevier.

Rider, M., & Kennedy, M. (2018). *The Geological Interpretation of Well Logs* (3 ed.). Rider-French Consulting Limited.

Schmidt, R. J. *Advanced mechanics of materials* (Vol. 6).

Stjern, G., Agle, A., & Horsrud, P. (2003). Local rock mechanical knowledge improves drilling performance in fractured formations at the Heidrun field. *Journal of Petroleum Science and Engineering, 38*(3-4), 83-96.

Zhang, J. (2013). Borehole stability analysis accounting for anisotropies in drilling to weak bedding planes. *International journal of rock mechanics and mining sciences, 60*, 160-170.

Aadnoy, B., & Looyeh, R. (2011). *Petroleum Rock Mechanics: Drilling Operations and Well Design*. Gulf Professional Publishing.

Aadnoy, B. S. (1998). Geomechanical analysis for deep-water drilling. IADC/SPE drilling conference,

Appendix

The formulas mentioned in literature directly depends on the models presented in the thesis. These equations are summarized in the table, with the variable dependent on the model on the right most column. The parameters are used for wellbore stability, geophysics, geomechanics and drilling operations.

Appendix A 1: Summary of application of this thesis work models

Parameters	Formula	Application of this thesis work
Pore pressure	$P_{pg} = OBG - (OBG - P_{ng})\left(\frac{\Delta t_n}{\Delta t}\right)^3$	Δt is the sonic transit time in shales obtained from well logging, OBG = overburden estimated from density log. However, this thesis work is applied for the OBG in the absence of density log and in the presence of sonic travel time from which density log can estimated from.
	$P_{pg} = OBG - (OBG - P_{ng})\left(\frac{R}{R_n}\right)^n$	Similarly, this thesis work is applied for the OBG in the absence of density log and in the presence of sonic travel time from which density log can estimated from. However, the resistivity log does not show good correlation with the density log
Overburden	$\sigma_v = \int_0^z \rho(z) * g\, dz$	$\rho(z)$= densety log In absence of density log and in the presence of sonic travel time, we use this thesis work model to estimate density from sonic log.
Internal friction angle	$sin\varphi = \frac{V_p - 1}{V_p + 1}$	$Vp = c$ompressional wave velocity modell In absence of sonic log and in the presence of density log, we use this thesis work model to estimate sonic log from density log.
Uniaxial compressive strength	$C_0 = 0{,}77 * v_p^{2,93}$	$Vp = co$mpressional wave velocity modell In absence of sonic log and in the presence of density log, we use this thesis work model to estimate sonic log from density log.
	$C_0(\text{MPa}) = 10\left(\frac{304.8}{\Delta t} - 1\right)$	Dt is sonic travel time, ms/ft The comment is similar to the one written above
Youngs modulus	$E = 0{,}076 v_p^{3,223}$	$Vp = c$ompressional wave velocity modell In absence of sonic log and in the presence of density log, we use this thesis model to estimate sonic log from density log.
Shear modulus	$G = 0{,}03 v_p^{3,3}$	$Vp = c$ompressional wave velocity modell In absence of sonic log and in the presence of density log, we use thesis work model to estimate sonic log from density log
Compressional wave velocity	$v_p = \sqrt{\frac{K + \frac{4}{3}G}{\rho}}$	In absence of density log and in the presence of sonic travel time, we use tis thesis work model to estimate density from sonic log. Vs can be determined from Vp. This thesis work model can be applied.
Shear wave velocity	$v_s = \sqrt{\frac{G}{\rho}}$	We use dens vs and Vp log. In the absence of one of the logs, we use this thesis work model to estimate.
Poisson's ratio	$v = \frac{\left(\frac{v_p}{v_s}\right)^2 - 2}{2\left[\left(\frac{v_p}{v_s}\right)^2 - 1\right]}$	In absence of density log and in the presence of sonic travel time, we use tis thesis work model to estimate density from sonic log. Vs can be determined from Vp. This thesis work model can be applied.
Horizontal stress	$\sigma_h = \frac{v}{1 - v}(\sigma_v - \alpha * P_p) + \alpha * P_p$	Density log and sonic logs are used to determine the Poisson's ratio, Pore pressure and overburden. In the absence of one of the logs, we use this thesis work models to estimate.

Table Table A1-A

Appendix A 2: All models developed in this thesis

Density – Compressional velocity

North Sea wells	Density – compressional velocity model		R^2
15-5-5	Linear	$\rho = 0{,}2479V_p + 1{,}4734$	$R^2 = 0{,}4688$
	Polynomial	$\rho = -0{,}1084V_p^2 + 0{,}8486V_p + 0{,}6658$	$R^2 = 0{,}4894$
	Power	$\rho = 1{,}5537\ V_p^{0{,}3263}$	$R^2 = 0{,}4578$
	Exponential	$\rho = 1{,}5546e^{0{,}1179Vp}$	$R^2 = 0{,}4388$
	Logarithmic	$\rho = 0{,}6833\ln(V_p) + 1{,}4747$	$R^2 = 0{,}4851$
15-6-12	Linear	$\rho = 0{,}0747\ V_p + 2{,}2665$	$R^2 = 0{,}4859$
	Polynomial	$\rho = -0{,}0442\ V_p^2 + 0{,}4249\ V_p + 1{,}5871$	$R^2 = 0{,}6677$
	Power	$\rho = 2{,}1644\ V_p^{0{,}1232}$	$R^2 = 0{,}5686$
	Exponential	$\rho = 2{,}275e^{0{,}0299\ Vp}$	$R^2 = 0{,}482$
	Logarithmic	$\rho = 0{,}3066\ln(V_p) + 2{,}1434$	$R^2 = 0{,}5693$
16-2-3	Linear	$\rho = 0{,}1558\ V_p + 1{,}8202$	$R^2 = 0{,}4244$
	Polynomial	$\rho = 0{,}1395\ V_p^2 - 0{,}8292\ V_p + 3{,}5254$	$R^2 = 0{,}5375$
	Power	$\rho = 1{,}8067\ V_p^{0{,}2166}$	$R^2 = 0{,}3829$
	Exponential	$\rho = 1{,}8772e^{0{,}0657\ Vp}$	$R^2 = 0{,}4226$
	Logarithmic	$\rho = 0{,}513\ln(V_p) + 1{,}73$	$R^2 = 0{,}384$
16-2-4	Linear	$\rho = 0{,}1681\ V_p + 1{,}7349$	$R^2 = 0{,}7961$
	Polynomial	$\rho = -0{,}0426\ V_p^2 + 0{,}4591\ V_p + 1{,}3067$	$R^2 = 0{,}8218$
	Power	$\rho = 1{,}743\ V_p^{0{,}2402}$	$R^2 = 0{,}7942$
	Exponential	$\rho = 1{,}7865e^{0{,}0739\ Vp}$	$R^2 = 0{,}768$
	Logarithmic	$\rho = 0{,}5457\ln(V_p) + 1{,}6798$	$R^2 = 0{,}8196$
16-2-6	Linear	$\rho = 0{,}2084\ V_p + 1{,}6635$	$R^2 = 0{,}6987$
	Polynomial	$\rho = -0{,}0627\ V_p^2 + 0{,}5958\ V_p + 1{,}1134$	$R^2 = 0{,}7405$
	Power	$\rho = 1{,}7003\ V_p^{0{,}2787}$	$R^2 = 0{,}7102$
	Exponential	$\rho = 1{,}7286e^{0{,}0924\ Vp}$	$R^2 = 0{,}6713$
	Logarithmic	$\rho = 0{,}6261\ln(V_p) + 1{,}6281$	$R^2 = 0{,}7344$
16-2-6T2	Linear	$\rho = 0{,}2078\ V_p + 1{,}6632$	$R^2 = 0{,}682$
	Polynomial	$\rho = -0{,}0552\ V_p^2 + 0{,}5485\ V_p + 1{,}1797$	$R^2 = 0{,}721$
	Power	$\rho = 1{,}701\ V_p^{0{,}2772}$	$R^2 = 0{,}693$
	Exponential	$\rho = 1{,}7275e^{0{,}0924\ Vp}$	$R^2 = 0{,}6542$
	Logarithmic	$\rho = 0{,}6212\ln(V_p) + 1{,}6303$	$R^2 = 0{,}7176$

Table A2-A

Norwegian Sea wells	Density – compressional velocity model		R^2
6608/10-17S	Linear	$y = 0{,}1347x + 2{,}0812$	$R^2 = 0{,}3284$
	Polynomial	$y = 0{,}0501x^2 - 0{,}1971x + 2{,}6218$	$R^2 = 0{,}3383$
	Power	$y = 2{,}0613x^{0{,}1706}$	$R^2 = 0{,}3209$
	Exponential	$y = 2{,}1223e^{0{,}0525x}$	$R^2 = 0{,}3247$
	Logarithmic	$y = 0{,}4365\ln(x) + 2{,}0078$	$R^2 = 0{,}3226$
6608/10-6	Linear	$y = 0{,}4694x + 0{,}9285$	$R^2 = 0{,}6208$
	Polynomial	$y = -0{,}1242x^2 + 1{,}1284x + 0{,}0734$	$R^2 = 0{,}6371$
	Power	$y = 1{,}2347x^{0{,}5809}$	$R^2 = 0{,}6377$
	Exponential	$y = 1{,}2019e^{0{,}2214x}$	$R^2 = 0{,}6162$
	Logarithmic	$y = 1{,}2248\ln(x) + 0{,}9921$	$R^2 = 0{,}6354$
6608/10-9	Linear	$y = 0{,}4137x + 1{,}1149$	$R^2 = 0{,}6222$
	Polynomial	$y = -0{,}1821x^2 + 1{,}3634x - 0{,}1002$	$R^2 = 0{,}6362$
	Power	$y = 1{,}3641x^{0{,}4967}$	$R^2 = 0{,}6349$
	Exponential	$y = 1{,}3272e^{0{,}1913x}$	$R^2 = 0{,}6227$
	Logarithmic	$y = 1{,}0721\ln(x) + 1{,}1762$	$R^2 = 0{,}632$

6406/11-1S	Linear	$y = 0,2501x + 1,6081$	$R^2 = 0,6498$
	Polynomial	$y = -0,1766x^2 + 1,294x + 0,1416$	$R^2 = 0,8017$
	Power	$y = 1,6552x^{0,3283}$	$R^2 = 0,7021$
	Exponential	$y = 1,6902e^{0,1101x}$	$R^2 = 0,6376$
	Logarithmic	$y = 0,744\ln(x) + 1,5619$	$R^2 = 0,713$

Table A2-B

Baren Sea wells	Density – compressional velocity model		R^2
7124-3-1	Linear	$y = 0,1405x + 1,9388$	$R^2 = 0,6554$
	Polynomial	$y = -0,0358x^2 + 0,4506x + 1,3225$	$R^2 = 0,7241$
	Power	$y = 1,8082x^{0,2386}$	$R^2 = 0,6756$
	Exponential	$y = 1,9825e^{0,0571x}$	$R^2 = 0,6215$
	Logarithmic	$y = 0,5842\ln(x) + 1,7168$	$R^2 = 0,7045$
7125-1-1	Linear	$y = 0,1742x + 1,8063$	$R^2 = 0,2949$
	Polynomial	$y = 0,025x^2 + 0,0166x + 2,0457$	$R^2 = 0,2969$
	Power	$y = 1,8215x^{0,2244}$	$R^2 = 0,2535$
	Exponential	$y = 1,8576e^{0,0742x}$	$R^2 = 0,2602$
	Logarithmic	$y = 0,5275\ln(x) + 1,7599$	$R^2 = 0,2875$
7324-6-1	Linear	$y = 0,0471x + 2,329$	$R^2 = 0,0464$
	Polynomial	$y = -0,0013x^2 + 0,0565x + 2,3117$	$R^2 = 0,0464$
	Power	$y = 2,2853x^{0,0695}$	$R^2 = 0,046$
	Exponential	$y = 2,3306e^{0,0192x}$	$R^2 = 0,0463$
	Logarithmic	$y = 0,1707\ln(x) + 2,2809$	$R^2 = 0,0461$
7324-7-2	Linear	$y = 0,0442x + 2,4161$	$R^2 = 0,0272$
	Polynomial	$y = 0,0566x^2 - 0,1487x + 2,5736$	$R^2 = 0,036$
	Power	$y = 2,456x^{0,0269}$	$R^2 = 0,0228$
	Exponential	$y = 2,4146e^{0,018x}$	$R^2 = 0,0268$
	Logarithmic	$y = 0,0664\ln(x) + 2,4579$	$R^2 = 0,0232$
7324-8-1	Linear	$y = 0,0422x + 2,326$	$R^2 = 0,0418$
	Polynomial	$y = 0,0488x^2 - 0,2524x + 2,7604$	$R^2 = 0,0712$
	Power	$y = 2,3362x^{0,0439}$	$R^2 = 0,0308$
	Exponential	$y = 2,3297e^{0,0168x}$	$R^2 = 0,0389$
	Logarithmic	$y = 0,1103\ln(x) + 2,3323$	$R^2 = 0,0334$

Table A2-C

Density – Shear velocity

North Sea wells	Density – Shear velocity model		R^2
15-6-12	Linear	$y = 0,1624x + 2,2162$	$R^2 = 0,3008$
	Polynomial	$y = -0,2373x^2 + 1,1282x + 1,2696$	$R^2 = 0,4751$
	Power	$y = 2,2893x^{0,1516}$	$R^2 = 0,3221$
	Exponential	$y = 2,2067e^{0,0697x}$	$R^2 = 0,2556$
	Logarithmic	$y = 0,3497\ln(x) + 2,3046$	$R^2 = 0,3712$
16-2-3	Linear	$y = 0,1517x + 2,0978$	$R^2 = 0,1358$
	Polynomial	$y = 0,3396x^2 - 1,0372x + 3,096$	$R^2 = 0,2442$
	Power	$y = 2,2465x^{0,0958}$	$R^2 = 0,1077$
	Exponential	$y = 2,1084e^{0,0645x}$	$R^2 = 0,1373$
	Logarithmic	$y = 0,2257\ln(x) + 2,2467$	$R^2 = 0,1069$
16-2-4	Linear	$y = 0,2333x + 1,9096$	$R^2 = 0,7479$
	Polynomial	$y = -0,0438x^2 + 0,3801x + 1,8205$	$R^2 = 0,7547$
	Power	$y = 2,1692x^{0,1483}$	$R^2 = 0,7153$
	Exponential	$y = 1,9293e^{0,1023x}$	$R^2 = 0,7198$
	Logarithmic	$y = 0,3379\ln(x) + 2,1768$	$R^2 = 0,742$
16-2-6	Linear	$y = 0,094x + 2,2214$	$R^2 = 0,2674$
	Polynomial	$y = 0,0337x^2 - 0,0196x + 2,3132$	$R^2 = 0,2744$
	Power	$y = 2,3077x^{0,0612}$	$R^2 = 0,2499$
	Exponential	$y = 2,2259e^{0,0395x}$	$R^2 = 0,2648$
	Logarithmic	$y = 0,1457\ln(x) + 2,3074$	$R^2 = 0,2519$
16-2-6T2	Linear	$y = 0,1306x + 2,1722$	$R^2 = 0,3604$
	Polynomial	$y = 0,0539x^2 - 0,0522x + 2,3163$	$R^2 = 0,3831$
	Power	$y = 2,297x^{0,0816}$	$R^2 = 0,3192$
	Exponential	$y = 2,1813e^{0,0543x}$	$R^2 = 0,3461$
	Logarithmic	$y = 0,1952\ln(x) + 2,2969$	$R^2 = 0,3291$

Table A2-D

Norwegian Sea wells	Density – shear velocity Model		R^2
6608/10-17S	Linear	$y = 0,1425x + 2,2753$	$R^2 = 0,2229$
	Polynomial	$y = -0,0377x^2 + 0,2688x + 2,173$	$R^2 = 0,2238$
	Power	$y = 2,3991x^{0,0924}$	$R^2 = 0,2267$
	Exponential	$y = 2,2891e^{0,0555x}$	$R^2 = 0,2204$
	Logarithmic	$y = 0,2364\ln(x) + 2,3961$	$R^2 = 0,2276$

Table A2-E

Baren Sea wells	Density – Shear velocity model		R^2
7324/8-1	Linear	$y = 0,0333x + 2,3877$	$R^2 = 0,0053$
	Polynomial	$y = 0,2265x^2 - 0,7066x + 2,9804$	$R^2 = 0,0461$
	Power	$y = 2,4226x^{0,0147}$	$R^2 = 0,0024$
	Exponential	$y = 2,3848e^{0,014x}$	$R^2 = 0,0054$
	Logarithmic	$y = 0,0348\ln(x) + 2,4252$	$R^2 = 0,0023$
7324/7-2	Linear	$y = 0,0442x + 2,4161$	$R^2 = 0,0272$
	Polynomial	$y = 0,0566x^2 - 0,1487x + 2,5736$	$R^2 = 0,036$
	Power	$y = 2,456x^{0,0269}$	$R^2 = 0,0228$
	Exponential	$y = 2,4146e^{0,018x}$	$R^2 = 0,0268$
	Logarithmic	$y = 0,0664\ln(x) + 2,4579$	$R^2 = 0,0232$
7324/6-1	Linear	$y = -0,0045x + 2,5091$	$R^2 = 0,0002$
	Polynomial	$y = -0,0339x^2 + 0,1276x + 2,3837$	$R^2 = 0,0029$
	Power	$y = 2,5014x^{-0,002}$	$R^2 = 5E-05$
	Exponential	$y = 2,5068e^{-0,002x}$	$R^2 = 0,0002$
	Logarithmic	$y = -0,005\ln(x) + 2,5033$	$R^2 = 7E-05$

Table A2-F

Compressional velocity - Shear velocity

North Sea wells	Compressional velocity - Shear velocity model model		R^2
15-6-12	Linear	$V_p = 1{,}5432V_s + 0{,}7982$	$R^2 = 0{,}9006$
	Polynomial	$V_p = -0{,}197\ V_s^{\ 2} + 2{,}3202\ V_s + 0{,}0669$	$R^2 = 0{,}9038$
	Power	$V_p = 2{,}2391\ V_s^{\ 0{,}7985}$	$R^2 = 0{,}9005$
	Exponential	$V_p = 1{,}6592e^{0{,}4174\ Vs}$	$R^2 = 0{,}877$
	Logarithmic	$V_p = 2{,}9137\ln(V_s) + 1{,}931$	$R^2 = 0{,}9008$
16-2-3	Linear	$V_p = 1{,}3645\ V_s + 1{,}0354$	$R^2 = 0{,}9218$
	Polynomial	$V_p = 0{,}3237\ V_s^{\ 2} + 0{,}3906\ V_s + 1{,}6615$	$R^2 = 0{,}9292$
	Power	$V_p = 2{,}4566\ V_s^{\ 0{,}615}$	$R^2 = 0{,}9342$
	Exponential	$V_p = 1{,}5192e^{0{,}4493\ Vs}$	$R^2 = 0{,}9468$
	Logarithmic	$V_p = 1{,}8462\ln(V_s) + 2{,}5069$	$R^2 = 0{,}889$
16-2-4	Linear	$V_p = 1{,}4181\ V_s + 1{,}0116$	$R^2 = 0{,}9838$
	Polynomial	$V_p = 0{,}04\ V_s^{\ 2} + 1{,}2842\ V_s + 1{,}0927$	$R^2 = 0{,}984$
	Power	$V_p = 2{,}4932\ V_s^{\ 0{,}6402}$	$R^2 = 0{,}9728$
	Exponential	$V_p = 1{,}5009e^{0{,}4426\ Vs}$	$R^2 = 0{,}9788$
	Logarithmic	$V_p = 2{,}0257\ln(V_s) + 2{,}6365$	$R^2 = 0{,}9537$
16-2-6	Linear	$V_p = 1{,}3036\ V_s + 1{,}208$	$R^2 = 0{,}8896$
	Polynomial	$V_p = 0{,}2138\ V_s^{\ 2} + 0{,}5595\ V_s + 1{,}8256$	$R^2 = 0{,}8954$
	Power	$V_p = 2{,}4863\ V_s^{\ 0{,}6122}$	$R^2 = 0{,}8762$
	Exponential	$V_p = 1{,}7867e^{0{,}3762\ Vs}$	$R^2 = 0{,}8947$
	Logarithmic	$V_p = 2{,}093\ln(V_s) + 2{,}3677$	$R^2 = 0{,}8484$
16-2-6T2	Linear	$V_p = 1{,}3832\ V_s + 1{,}1056$	$R^2 = 0{,}9402$
	Polynomial	$V_p = 0{,}26\ V_s^{\ 2} + 0{,}459\ V_s + 1{,}8635$	$R^2 = 0{,}9538$
	Power	$V_p = 2{,}4932\ V_s^{\ 0{,}6268}$	$R^2 = 0{,}9271$
	Exponential	$V_p = 1{,}7478e^{0{,}3898\ Vs}$	$R^2 = 0{,}952$
	Logarithmic	$V_p = 2{,}1732\ln(V_s) + 2{,}3892$	$R^2 = 0{,}8739$

Table A2-G

Norwegian Sea wells	Compressional velocity - Shear velocity model model		R^2
6608/10-17S	Linear	$y = 1{,}2537x + 1{,}1489$	$R^2 = 0{,}9566$
	Polynomial	$y = 0{,}3413x^2 + 0{,}1363x + 2{,}0288$	$R^2 = 0{,}9622$
	Power	$y = 2{,}3632x^{0{,}6213}$	$R^2 = 0{,}9582$
	Exponential	$y = 1{,}6727e^{0{,}3914x}$	$R^2 = 0{,}9664$
	Logarithmic	$y = 1{,}9793\ln(x) + 2{,}2599$	$R^2 = 0{,}9381$

Table A2-H

Barenes Sea wells	Compressional velocity - Shear velocity model model		R^2
7324/8-1	Linear	$y = 1{,}2162x + 1{,}1862$	$R^2 = 0{,}7092$
	Polynomial	$y = 0{,}3858x^2 - 0{,}0341x + 2{,}1783$	$R^2 = 0{,}7216$
	Power	$y = 2{,}3806x^{0{,}586}$	$R^2 = 0{,}7132$
	Exponential	$y = 1{,}6954e^{0{,}3803x}$	$R^2 = 0{,}7329$
	Logarithmic	$y = 1{,}8547\ln(x) + 2{,}2808$	$R^2 = 0{,}676$
7324/7-2	Linear	$y = 1{,}2534x + 1{,}1526$	$R^2 = 0{,}9337$
	Polynomial	$y = 0{,}0361x^2 + 1{,}1226x + 1{,}2659$	$R^2 = 0{,}9339$
	Power	$y = 2{,}355x^{0{,}6383}$	$R^2 = 0{,}9327$
	Exponential	$y = 1{,}7281e^{0{,}3715x}$	$R^2 = 0{,}9342$
	Logarithmic	$y = 2{,}1283\ln(x) + 2{,}2125$	$R^2 = 0{,}9104$
7324/6-1	Linear	$y = 1{,}182x + 1{,}3092$	$R^2 = 0{,}804$
	Polynomial	$y = -0{,}0144x^2 + 1{,}238x + 1{,}2562$	$R^2 = 0{,}804$
	Power	$y = 2{,}3871x^{0{,}6239}$	$R^2 = 0{,}8315$
	Exponential	$y = 1{,}8862e^{0{,}3304x}$	$R^2 = 0{,}8242$
	Logarithmic	$y = 2{,}2104\ln(x) + 2{,}1658$	$R^2 = 0{,}7957$

Table A2-I

Multivariate Density and Compressional velocity

North Sea wells	Multivariate model		R	
16-2-3	Multivariate VP	Y=-1,24503983465011 +1,09684128660379*VS+1,26285506483481*DEN+-0,984812412392818*por	Multiple R	0,982552039044441
			R- squared	0,965408509430389
			adjusted R-squared	0,965314083159498
			Standard error	0,0779005863332837
			Observations	1103
	Multivariate DEN	Y=2,49303316915152+-0,364520653041707*VP+-1,11506204428424*VS+0,235156029285666*por	Multiple R	0,950114168906911
			R- squared	0,902716933957669
			adjusted R-squared	0,902451375087672
			Standard error	0,0336156900304174
			Observations	1103
16-2-4	Multivariate VP	Y=0,155316580102066+1,15671991478187*VS+0,637287100100291*DEN+-0,582653091257998*por	Multiple R	0,994970240328101
			R- squared	0,989965779138558
			adjusted R-squared	0,989962264114903
			Standard error	0,0952128017256032
			Observations	8568
	Multivariate DEN	Y=1,80194322076851+0,360277527200761*VP+-0,358431957912963*VS+-0,411843384213626*por	Multiple R	0,916733956585633
			R- squared	0,840401147157148
			adjusted R-squared	0,840345239105008
			Standard error	0,0715890118224086
			Observations	8568
16-2-6	Multivariate VP	Y=-1,82480384354745+1,13544687429682*VS+1,47330923189265*DEN+-0,996987726607551*por	Multiple R	0,96700150514351
			R- squared	0,935091910949814
			adjusted R-squared	0,934966201287355
			Standard error	0,125323130895258
			Observations	1553
	Multivariate DEN	Y=2,43869622117695+0,110842867396058*VP+-0,155248397018799*VS+-0,765777858868633*por	Multiple R	0,823719231483958
			R- squared	0,678513372316522
			adjusted R-squared	0,67789073843463
			Standard error	0,0343746398808144
			Observations	1553
16-2-6T2	Multivariate VP	Y= -1,03710912256709 + 1,20729369004553 *VS+ 1,02794623895715 *DEN+ -0,157899944304357 *por	Multiple R	0,976408862291522
			R- squared	0,953374266361425
			adjusted R-squared	0,953323714427592
			Standard error	0,134388355931144
			Observations	2771
	Multivariate DEN	Y= 2,24853415988056+ 0,211196785553098*VP -0,257235886704363*VS -0,603497224096615*por	Multiple R	0,771643794531946
			R- squared	0,59543414563966
			adjusted R-squared	0,594995512620838
			Standard error	0,0609144169886344
			Observations	2771

Table A2-J

Well Barents Sea	Multivariable model		*Regresjonsstatistikk*	
7374/7-2	Velocity	Vp = a+bVs+ c*ρ+d*φ a= -0.994025557751479 d- 0.101369776327267 *Vs b=+ 1,17697879767033*DEN c=+ 0.919461526349866 *POR	Multiple R	0,98122005
			R- squared	0,96279278
			adjusted R-squared	0,96277713
			Standard error	0,09303758
			Observations	7137
	Density	ρ = a+bVp+ c*Vs +d*φ a=1,66635205340664 b= + 0,455362644344926*Vp c= - 0,450285896817343* Vs d= + 0,388330919745864*POR	Multiple R	0,69830504
			R- squared	0,48762993
			adjusted R-squared	0,48741444
			Standard error	0,06547422
			Observations	7137
7324/8-1	Velocity	Vp = a+bVS+ c*ρ+d*φ a=- 0,938695853413405 d=+ 0,95751256609354*Vs b= + 1,15710627868627DEN c=– 1,11223275829274*POR	Multiple R	0,90155606
			R- squared	0,81280332
			adjusted R-squared	0,81249543
			Standard error	0,14295723
			Observations	1828
	Density	ρ = a+bVp+ c*Vs +d*φ a= 1,45536816874572 b=+ 0,318715101439793*Vp c= -0,161966293220614*Vs d= + 0,960012038037819*POR	Multiple R	0,68995496
			R- squared	0,47603785
			adjusted R-squared	0,47517607
			Standard error	0,07502756
			Observations	1828
7324/6-1	Velocity	Vp = a+bVS+ c*ρ+d*φ a= -0,994025557751479 d=– 0,101369776327267*Vs b=+ 1,17967879767033*DEN c=+ 0,919461526349866*POR	Multiple R	0,948609531
			R- squared	0,899860042
			adjusted R-squared	0,899800518
			Standard error	0,125889833
			Observations	5051
	Density	ρ = a+bVp+ c*Vs +d*φ a=1.38075780450407 b= + 0.332332620356815*Vp c= -0.223178134178637* Vs d= + 1.25895161558018*POR	Multiple R	0,679581203
			R- squared	0,461830611
			adjusted R-squared	0,461510717
			Standard error	0,063944988
			Observations	5051

Table A2-K

Appendix A 3: Best models with higher R^2 value

The best regression models, in terms of the avrage error percentage for all the wells available in this thesis, are presented below. The two leftmost columns is the variable input and output, and the top row is area of interest.

Input information	Output information	North Sea	Norwegian sea	Baren sea	Norwegian continental plate
Vs	Vp	Eq 4.32	Eq 4.41	Eq 4.41	Eq 4.41
Vp	Den	Gardner eq 2.28	Eq 4.10	Eq 4.11	Eq 4.11
Vs	Den	Eq 4.19	AnbazhagenEq 2.32	Eq 4.27	Anbazhagen Eq 2.33
Por, Vp & Vs	Den	Eq 4.44	x	Eq. 4.46	x
Por, Vs & Den	Vp	Eq 4.45	x	Eq 4.51	x

Table A3-A